The Pennsylvania State University

The Graduate School

IMPACT OF ATOMIZATION GAS ON CHARACTERISTICS OF STAINLESS STEEL POWDER FEEDSTOCKS FOR ADDITIVE MANUFACTURING

A Thesis in

Engineering Science and Mechanics

by

Mingze Gao

Submitted in Partial Fulfillment

of the Requirement

for the Degree of

Master of Science

May 2020

The thesis of Mingze Gao was reviewed and approved by the following:

Todd A. Palmer
Professor of Engineering Science and Mechanics
Professor of Material Science and Engineering
Thesis Advisor

Andrea Paola Arguelles
Assistant Professor of Engineering Science and Mechanics

Jayme S. Keist
Assistant Professor of Material Science and Engineering

Reginald F. Hamilton
Associate Professor of Engineering Science & Mechanic

Judith A. Todd
Department Head and P.B. Breneman Chair of Engineering Science & Mechanics
Professor of Engineering Science & Mechanics

Bellamarie Ludwig
Assistant Research Professor of Applied Research Laboratory
Special Signatory

ABSTRACT

Powders are primary feedstock materials for most of additive manufacturing processes. The characteristics of powder are essential for bulk powder behaviors, such as flow and packing, and can eventually impact the quality of the fabricated components. Even though the characteristics of powder are closely related to its atomization conditions, the impact of atomization gas on the powder characteristics has not been sufficiently studied. The characteristics of three 316L austenitic stainless-steel powders, gas atomized with nitrogen or argon, were investigated. The particle size distributions of the powders are nearly identical. Even though there is no obvious difference in SEM images of the powders, particle morphology was quantified in details, such as convexity, aspect ratio and circularity, to explore if there are subtle differences in the powders. Convexity and circularity showed no considerable difference. Compared with nitrogen atomized powders, argon atomized powder has 10% more particles with aspect ratio close to one, which indicates there are 10% more highly spherical particles in argon atomized powder. Particles were found to be less spherical as the particle size increases from 10 to 35μm, and this trend is observed on all the powder samples. Traditional powder packing measurements, apparent density and tap density, indicated that argon atomized powder exhibits slightly higher packing density compared with nitrogen atomized powders. Even though traditional flowability measurements, flow rate and angle of repose, showed no difference in the powders, rheological flowability measurements showed considerable differences. Argon atomized powder showed 5 degrees lower avalanche angle, which can be correlated to the 10% more highly spherical particles. It was also demonstrated that particles with lower aspect ratio exhibit higher interparticle force by numerical simulations. Internal porosity in powder particles was found to impact basic flow energy measurements. Due to the exist of internal porosity, the true volume of the powder is reduced, and

less energy is needed to keep the powder flowing. The local void size distribution of powder bed was accessed by micro-CT. Permeability of powder bed tends to be more dependent on the local void size than bulk packing density, and the difference in local void size can be correlated to a small difference in particle size.

TABLE OF CONTENTS

LIST OF FIGURES

LIST OF TABLES

ACKNOWLEGEMENTS

I would like to thank first and foremost my advisor Dr. Todd Palmer for providing the opportunity to perform this research and also providing me helpful advice through meetings. Thanks to his support and guidance through this work, I can learn to improve my academic skills. Also, I am extremely grateful to be in the research group with many enthusiastic and helpful members, Andrew Iams, Titus Reed, Dereck Shaffer, Selda Nayir and Skyler Hilburn. They are not only perfect teammates, but also nice friends.

I am grateful to Dr. Bellamarie Ludwig for helping me with conducting powder rheometer measurements and answering me the questions I have on the results. I thank Mr. Timothy Stecko for his time and patience on helping me with micro-CT scanning and training me on data processing. I also thank Dr. Ekaterina Bazilevskaya for training me on Malvern Morphologi G3SE system for particle characterization. I also thank Dr. Andrea Paola Arguelles, Dr. Jayme S. Keist and Dr. Reginald F. Hamilton for serving on the committee and valuable comments on my thesis.

Finally, I would like to thank my parents for their supporting and understanding. Thanks to their encouraging, I can continue my education in one of the best universities in the world and achieve my future goals.

Chapter 1

Introduction

1.1 Feedstock Materials for Additive Manufacturing

Additive manufacturing (AM) processes, which utilize a layer-by-layer build methodology, are growing in popularity, in part, because of their ability to produce complex geometries across a range of metallic material systems [1], [2]. These processes, which include laser and electron beam-based powder bed fusion (PBF) and binder jet printing, utilize metal powders as the primary feedstock material. The characteristics of the powder are essential to the bulk powder properties, such as flow and packing, and might impact the effectiveness of powder recoating processes and further affect the quality of the final parts. Powders can be produced by different atomization methods, such as gas atomization, plasma rotating electrode process and plasma atomization, as shown in Fig. 1-1. Resulting from the different atomization conditions, the properties of metal powders might vary, such as particle size distribution (PSD), particle morphology and chemical composition. Fig. 1-2 showed Ti-6Al-4V powders atomized by three primary atomization processes, gas atomization (GA), plasma rotating electrode process (PREP) and plasma atomization (PA). Generally, GA powder particles are close to spherical, with slightly deviating from perfect spheres and a few satellites. PREP powder particles, as shown in Fig. 1-2 (b), are perfectly spherical and typically larger in particle size. By contrast, PA powder particles are smaller and mostly spherical with a few satellites.

In powder bed fusion (PBF) processes, metal powders with particle sizes typically between 20 μm and 60 μm in diameter are spread in a thin layer, which is several particles in thickness, using a blade or roller [1]. Given the complexity of this spreading process, the beam-material

interactions governing the fusion-based PBF processes can be affected by the ability of powders to flow and form dense packing, thus impacting the properties of the as-built components. Machine manufacturers try to minimize these potential variations in powder spreading by specifying a narrow size range or particle size distribution (PSD) for metal powder feedstocks, particularly for PBF applications [3]. Table 1-1 shows the general particle size ranges.

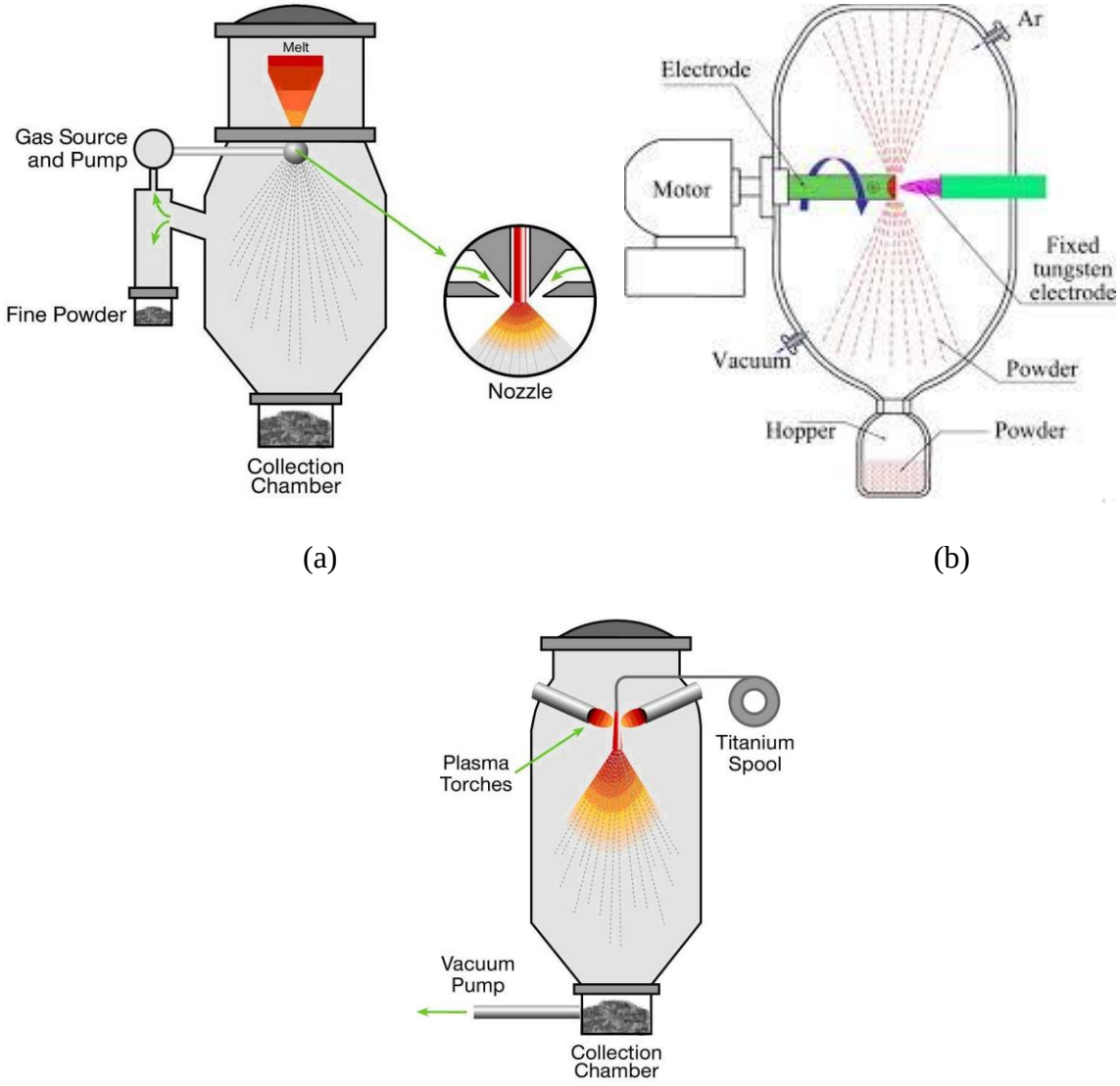

Fig. 1-1 Primary powder atomization methods, including (a) gas atomization [4], (b) plasma rotating electrode process (PREP) [5] and, (c) plasma atomization [4]

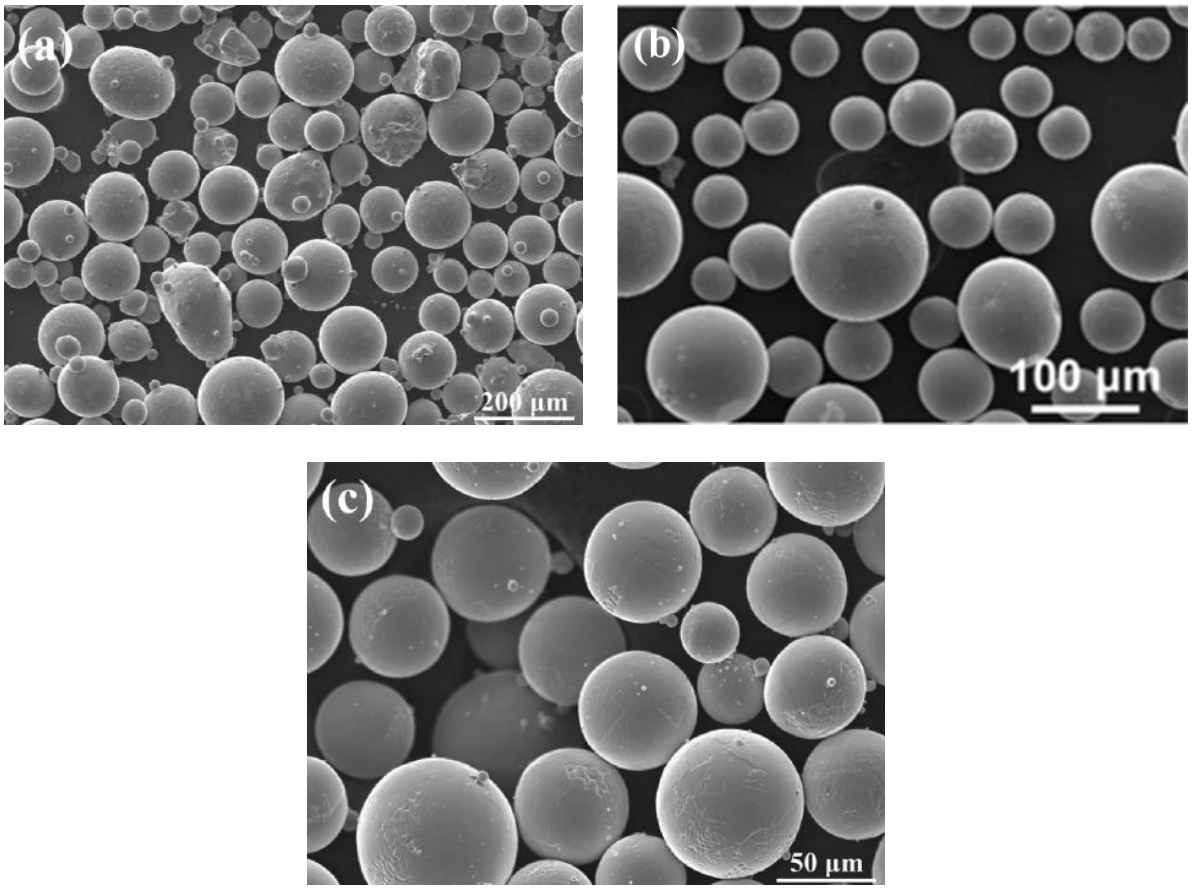

Fig. 1-2 Micrographs of Ti-6Al-4V powders atomized by

(a) GA [6], (b) PREP [7], and (c) PA [6]

Table 1-1 Typical particle size ranges used in different powder bed based AM processes

Process	Typical particle size (µm)
Laser Beam Melting	15-63
Electron Beam Melting	45-105
Binder jetting Printing	< 25

Traditionally, powder characterization for AM process mainly focused on the measurement of particle size distribution. However, even with the rather tight PSD requirements typically

imposed on AM feedstocks, the interactions between individual powder particles during spreading are dependent on a range of other particle properties that are not captured by PSD alone. Table 1-2 summarizes primary powder characteristics and typical metrology methods that are used to measure them. For example, particle morphology, packing density and flowability, which are generally not well characterized or measured, can also impact manufacturing process and the quality of the fabricated components [8-10].

Table 1-2 Typical metrology methods used for powder characterization

Powder Characteristics	**Metrology Methods**
Particle size distribution	Laser diffraction [11] [12] [13]
	Image analysis [14] [15] [16]
Particle morphology	Scanning electron microscopy [11] [12] [13]
	Image analysis [14] [17] [18]
Bulk chemical composition	Inductively Coupled Plasma [11] [12] [19]
Surface chemical composition	Auger spectroscopy [19]
	X-ray photoelectron spectroscopy [19] [20]
	Energy dispersive X-ray (EDX) [12]
Particle surface roughness	Atomic force microscopy [19]
	Confocal laser scanning microscopy [19]
Surface energy	Inverse gas chromatography [21]
True density	Helium Pycnometer [15] [19] [20]
Internal porosity	X-ray computer tomography (μCT) [18] [19] [22]

For example, in laser-based PBF processes, properties of the metal powders can impact the packing of the particles on the powder bed and affect the thermal conductivity and laser absorptivity between particles [8], [9]. Other characteristics, such as flowability, affect the consistency of the interactions between the powder feedstock and the recoating system, resulting in non-uniform powder packing, which might lead to the high surface roughness and low dimensional accuracy [10].

1.2 Traditional Powder Characterization and Powder Rheology

In traditional press and sinter powder metallurgy (PM) applications, besides particle size distribution measurements, other techniques commonly used to characterize the packing density and interparticle friction of powder particles can be used to characterize metal powders for AM [23]. These techniques, which are primarily directed at identifying the ability of metal powder particles to flow and fill a mold in a consistent manner, include the apparent density [24], tap density [25], angle of repose, and flow rate [26]. While these traditional techniques can provide important insight into the properties of individual powder lots, previous investigations have shown that they have limited applicability to characteristics in powder spreading in PBF applications [27].

Powder rheology is the study of properties and characteristics of powder, such as flowability, shear property and permeability, when the powder acts like a liquid or “soft solid”. Recent innovations have led to the development of new rheology-based tools, which utilize modern techniques, such as image analysis or sensors [27]. By the assistance of modern techniques, results are obtained automatically, which minimizes the errors from operators, and also subtle differences in powders can be identified. Table 1-3 summarizes typical powder rheological tools and the relative measurements on powders.

Table 1-3 Typical metrology methods used for powder rheological measurements

Metrology Methods	**Powder Rheological Measurements**
Rotating drum	Flowability [11] [12] [15]
Powder rheometer	Flowability [11] [13] [14]
	Fluidization [11] [13] [23]
	Compressibility [13] [24]
	Permeability [13] [24]
Shear cell	Shear property [11] [14] [15]
Heap shape method	Static angle of repose [12] [21]

Compared to traditional powder characterization, modern powder rheological tools, characterize bulk powder properties under different conditions. Rotating drum method, employed by Revolution Powder Analyzer (Mercury Scientific Inc. of Newtown, CT) and Granudrum® (Granutools™, Awans, Belgium), evaluates flowability by monitoring the avalanche behavior of powders as the drum is rotating. This method uses a digital camera to capture the geometry of the avalanche of the powders in the drum, and image analysis is employed to analyze the behaviors of powders during the building, peak, and minimum stages of the avalanche cycle. Another widely used powder rheological technique is powder rheometer, employed by the FT4 powder rheometer (Freeman Technology Ltd., Tewkesbury). In this method, there is an impeller moving into a powder bed with both translational and rotational motions. The force and torque on the impeller will be measured. The flow energy is calculated by the summation of the rotational and translational work required to move the impeller a certain distance into a powder bed. Shear cell measures the shear stress needed to move a powder sample under a range of normal stresses. With

the help of Mohr's circles of stress, cohesion and many other parameters can be determined. In the heap shape method, employed by the GranuHeap® (Granutools™, Awans, Belgium), a powder heap is created on a cylindrical support, and the geometry of the head will be measured by image analysis.

1.3 Objective

As interest in the use of AM processes for critical applications and more complex geometries is growing, the impact of metal powder feedstocks on the final component properties is becoming a more important consideration to both designers and end users. For example, changes in powder composition have a distinct impact on the properties of as-deposited and post-processed nickel-based alloys and stainless steel [28], [29]. Powders of nominally the same material with difference in nitrogen concentration, resulting from different atomization gases, nitrogen or argon, eventually resulted in significant different AM responses [29]. On the other hand, powder characteristics are largely determined by the atomization methods. As shown in Fig. 1-2, powders of nominally the same material, produced by different atomization methods, can be very different. This variation will result in inconsistent powder behaviors and further impact the in-process performance and the quality of fabricated components. Concerning this, the selection of argon or nitrogen as the primary atomization gas might also impact powder characteristics, which has not been explored yet.

The objective of the current work is to investigate the impact of nitrogen or argon as atomization gas on the powder characteristics, and employ experimental and numerical tools to investigate how the difference in powder characteristics impact rheological response. A range of traditional powder characterization tools and new rheology-based techniques were employed. Typical powder rheology tools, rotating drum method, powder rheometer and shear cell, were used

to evaluate rheological performance. Numerical simulations were conducted to elucidate the microscopic particle interactions. This work would enhance the understanding of the impact of atomization gas (nitrogen or argon) on powder characteristics and its relation to rheological performance. The obtained information would help predict powder behaviors and powder bed properties in AM processes. The following steps are needed, and special attention would be paid to the comparison of nitrogen or argon atomized powders.

- Characterize the powder samples. Besides particle size determination, other powder characteristics, such as particle morphology, will be quantified in details.
- Evaluate powder rheological properties. Besides traditional powder characterization, a range of powder rheological measurements will to be conducted, employing rotating drum method, powder rheometer and shear cell. The physical meanings of the obtained parameters will be discussed in details.
- Correlate powder characteristics to rheological response. The reasons for the difference in rheological performance of powders will be identified by correlating it to the basic powder characteristics.
- Numerical simulation of the rotating drum method. Microscopic particle interactions will be elucidated with numerical simulations.

1.4 Outline of Thesis

Chapter 2 reviews the existing research on standard and non-standard characterizations of powder properties. It begins with ASTM standards for powder characterization of different categories. The investigations of the impact of powder characteristics on the rheological

measurements are then summarized. Both experimental and numerical work on powder rheology are reviewed. The gap of knowledge and challenges for future work are identified.

Chapter 3 covers the powder materials, and the measurements of basic powder characteristics made on the powder samples. Differences in powder characteristics of powder samples are identified. The results of traditional powder characterizations will be discussed.

Chapter 4 describes the experiments of rotating drum method. The results are discussed in details and a correlation is made between rheological performance and powder characteristics. Numerical simulations of rotating drum method are conducted to elucidate the particle interactions.

Chapter 5 provides the experiments of powder rheometer and shear cell. The results are discussed in details and a correlation is made between rheological performance and powder characteristics.

Summary and conclusion are then provided in Chapter 6.

Chapter 2

Literature Review

Existing research on powder characterization and powder rheology was reviewed with respect to this work. Numerous standardized powder characterization tools, which are available for characterizing metal powders for AM, will be briefly described. Besides the existing standards, other new rheology-based techniques are also increasingly used to characterize powders. There are attempts to correlate powder characteristics to rheological responses. The role of particle size distribution has been addressed for many years, while other powder characteristics are also being studied. These differences in powder characteristics are mainly from different atomization conditions or recycling. Numerical simulations were also conducted for a better understanding of particle interactions.

2.1 ASTM Standards

A variety of ASTM Standards exist for different powder characterizations, including particle size determination, morphology determination, packing density, flow characteristics and chemical composition [30]. The referenced documents were classified in Table 2-1. As shown in Table 2-1, particle size determination tests, sieving and light scattering, both have applicable range of particle size. In standard B214, the particle size is determined by simply sieving with openings from 45 to 1000 μm and therefore not suitable for powders with particles smaller than 45 μm in diameter. By contrast, light scattering in standard B822 is capable of determining the particle size ranging from 0.4 μm to 2 mm. Another widely used technique for particle size determination is image analysis, which has not been standardized yet. Particle morphology was defined in standard

Table 2-1 Powder characterization standards in ASTM F3049

Particle size determination	B214 Sieving; range: 45 to 1000 μm
	B822 Lighting scattering; range: 0.4μm to 2mm
	Non-standardized: image analysis
Morphology determination	B243 Define powder shapes
	Non-standardized: light scattering and image analysis
Density and packing	B212 Determine apparent density by Hall flowmeter funnel
	B417 Determining apparent density by Carney funnel
	B329 Determine apparent density by Scott Volumeter
	B703 Determine apparent density by Arnold meter
	B527 Determine the tap density
	B923 Obtaining the skeletal density of metal powders
Flow characteristics	B213 Determine the mass flow rate by Hall flowmeter funnel
	B964 Determine the mass flow rate by Carney funnel
	B855 Determine the volume flow rate by Hall flowmeter funnel
Chemical Composition	E1447 Determine the hydrogen content in solid titanium and titanium alloys
	E1569 Determine the oxygen content in tantalum powder
	E1941 Determine carbon content in refractory and reactive metals
	E2371 Determine the content of elements other than oxygen, nitrogen, hydrogen and carbon in titanium and titanium alloys
	E2792 Determine the hydrogen content in solid aluminum and aluminum alloy

B243 and can be determined by light scattering and image analysis, however, no standards describe a means of quantifying it. Packing density of powder can be measured based on numerous standards, such as B212, B417, B329 and B703. Different standards employ different funnels with different geometries, and each of them is readily applicable to metal powders for additive manufacturing. Flow characteristics can be obtained with standards B213, B964 and B855 by measuring the flow rate with different flowmeters. It is worth to mention that these methods may not be suitable for the powders with irregular shape or with significant fraction of fine particles, which might be non-free flowing powders. For chemistry composition, several techniques such as inert gas fusion, atomic emission plasma spectrometry and combustion analysis are employed to analysis the element content like oxygen, hydrogen and carbon in different alloy system.

These testing methods mentioned in the standards provide convenient and reliable ways to characterize basic powder properties. However, because of the complexity of additive manufacturing processes, these tests are insufficient to capture powder interactions that powders would experience in additive manufacturing process. Powder rheology has been proved to be able to capture subtle differences of powders that traditional powder characterizations could not capture [27].

2.2 Impact of Powder Characteristics on Rheological Properties

Basic powder properties, such as particle size distribution, particle shape, chemical composition and flow characteristics, can be obtained using the testing methods in ASTM F3049. However, due to the complexity of additive manufacturing processes, a deeper understanding of the physics behind the interaction of powder particles is needed. It is essential to investigate how these powder characteristics would influence powder interactions by employing powder rheology.

Particle size distribution, as one of the most important powder properties, has been shown to greatly impact powder interactions and further influence rheological response [12], [31-33]. Different particle size distributions (small-sized or coarse-sized powders) of Ti-45Nb, Ti-18Nb-11Zr and Ni-Ti powders were characterized with three different powder characterization tools, heap shape method, rotating drum method and tapped density method, in order to compare the flowability of the powders [12]. Coarse-sized (45-100 μm) powders exhibit considerably lower angle of repose and negligible cohesiveness compare to small-sized powders (smaller than 45 μm). When particle size decreases, the effect of cohesive force gets stronger, as the gravity force decreases drastically with the decrease in particle size. For the particles smaller than 45 μm, cohesive force is dominant over gravity force, which inhibits the free flowing of powder particles.

Besides flowability, particle size distribution can also influence powder packing behaviors. For example, it has been shown that in binder jetting additive manufacturing process, the use of bimodal powder mixtures, compared to mono-sized powders, increased the powder packing density [33], as shown in Fig. 2-1. In this work, the ratio of the size of the coarse and fine particles were within 3:1 to 6:1, and in the bimodal powder mixture, the ratio of the coarse-sized and fine-sized particles by weight was 73:27. Generally, larger particle size will result in larger void space. For bimodal powder mixture, the fine powder particles could fit in the void space between larger particles, which contributes to a denser packing. The difference in packing density was observed in apparent density, tap density and also the density of greet part.

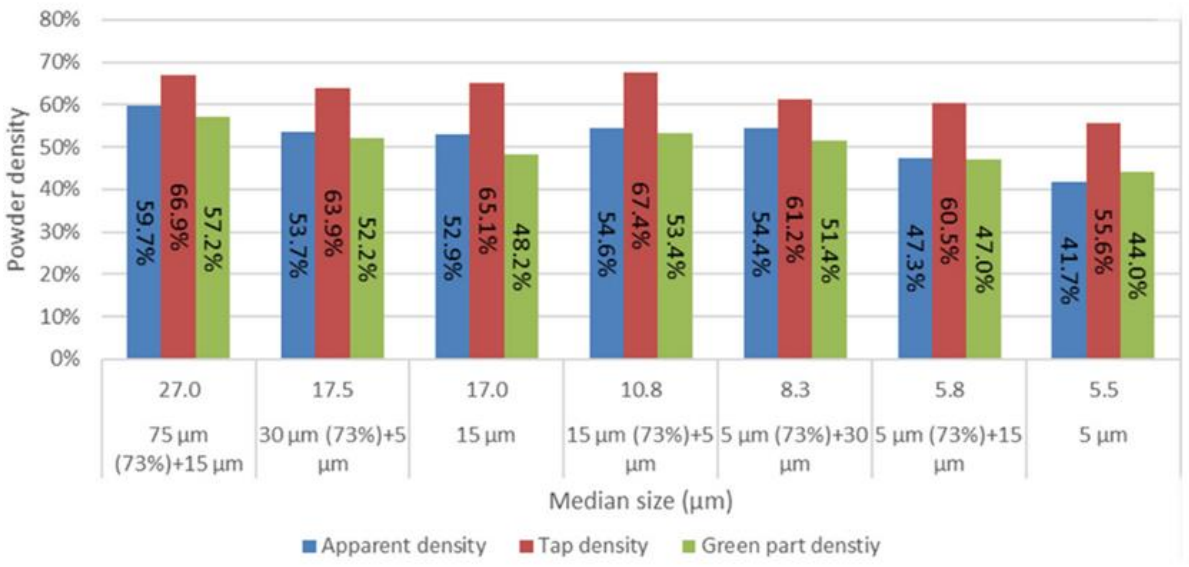

Fig. 2-1 Comparison of apparent, tap, and green density for different powder mixtures [33]

Particle shape is largely dependent on powder fabrication route, such as gas or water atomization, and the impact of it on rheological performance of powders is also explored [11], [34], [35]. For example, gas and water atomized 17-4PH stainless steel metal injection molding feedstocks were compared in terms of critical solid loading, viscosity and mixing torque measured by Haake PolyLab torque rheometer and capillary rheometer [35]. It was found that gas or water atomized powders behave differently under these rheological processes, which is believed to be influenced by the difference in particle morphology.

In another case, powders produced through plasma atomization (PA) and inert gas atomization (IGA) have been characterized and compared to identify differences arising from the different powder production processes [11]. The powder from inert gas atomization showed mostly spherical but deformed surface, while powder from plasma atomization has a precisely spherical morphology, as shown in Fig. 2-2. Flowability of the powders was compared by a range of techniques, such as packing density, angle of repose, revolution powder analyzer and FT4 powder rheometer. With more spherical particles, powder from PA exhibited considerably higher

flowability, as indicated by lower angle of repose, avalanche angle and flow energy, and higher packing density.

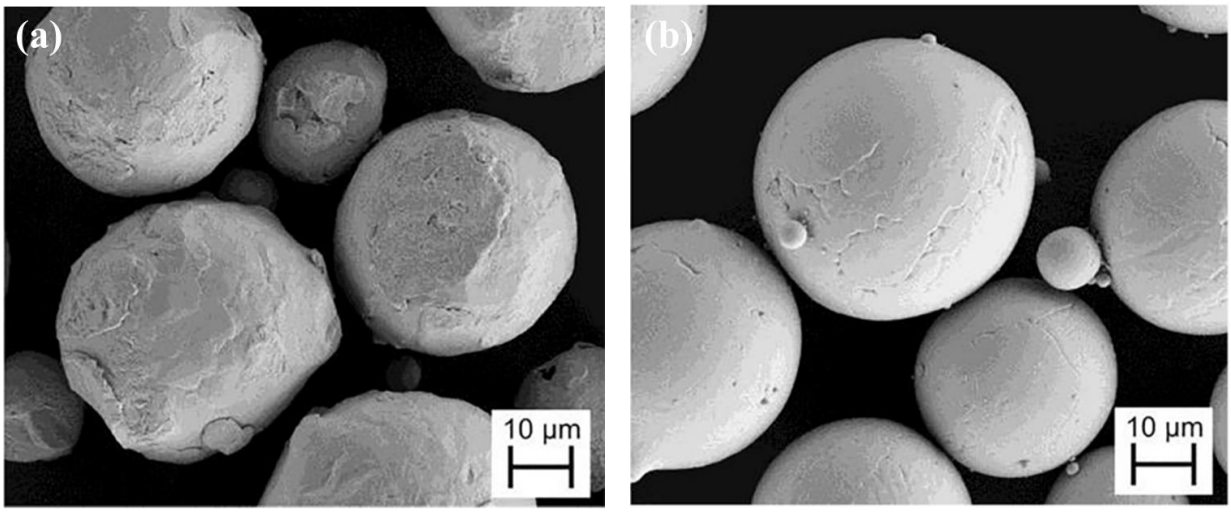

Fig. 2-2 SEM images of (a) IGA and (b) PA powder morphology [11]

Particle interactions are greatly impacted by particle shape. For example, the rotation of particles contributes a lot to the flow of powders. Spherical particles do not need additional free space in the surrounding volume when rotating, while irregular-shaped particles need more space, which increases the interlocking with surrounding particles. For the same reason, irregular-shaped particles result in lower packing efficiency compared with spherical particles.

Previous work has shown that there are some correlations between morphology of powder particles and the rheological performance, however, most of the work differentiated the particle morphology through observation, for instance, SEM images. In fact, observation only works when the difference in particle morphology is large enough to be captured by human eyes, while it is not uncommon that powders have subtly different morphologies. In that case, a detailed quantification is needed to capture the subtle difference in particle morphology. Modern image analysis technique allows more detailed quantification of particle morphology, such as Malvern Morphologi 3D

system, which has been used to characterize the shape of powder particles [18]. With high resolution image analysis technique, it would be interesting to investigate if small difference in particle morphology impacts rheological response.

Cohesion of powders has attracted much attention over many years because of its complexity and significant impact on rheology [21], [36-38]. Investigating cohesion is challenging because there are many interparticle forces involve, such as van der Waals force, electrostatic force, local chemical bonds or even surface liquid capillary attraction if in high humidity environment. Strong cohesion effect is usually observed on fine powders, as the gravity force decreases drastically with the decrease in particle size, which makes cohesive force dominates over it, and that is also the reason that cohesion effect is strongly dependent on particle size. Avalanching flow of cohesionless glass beads and cohesive powders were compared with rotating drum method, and it was found that the avalanching dynamics of cohesive powders is substantially different from those observed for cohesionless glass beads [37]. Different from free-flowing glass beads, cohesive powder exhibits history-dependent flow dynamics and aperiodic avalanche frequencies. It is obvious that increase in cohesiveness of powder makes the powder behaviors less predictable.

Cohesiveness was quantified with surface energy and cohesive index by inverse gas chromatography (IGC) and Granudrum® (Granutools™, Awans, Belgium), respectively [21]. It was found that high cohesiveness, resulting from the presence of more fines, considerably decreases flowability, as indicated by higher angle of repose, lower flow rate and packing density. Indeed, cohesion would lead to agglomeration, due to interparticle attraction force, which inhibits the free-flowing of powder particles and decreases packing efficiency.

There was also an attempt to measure the cohesive force with atomic force microscopy (AFM) by measuring the pull-off force between powder particles [38]. The pull-off forces of ten combinations of six powders were measured, and each combination was measured 100 times, as shown in Fig. 2-3. The flowability of the powders were evaluated by bin-flow test, and the details of bin-flow test could be found in [38]. Based on the flowability results from bin-flow test, the powders that exhibit higher pull-off force also exhibit poor flowability, which means that pull-off adhesion force plays an important role in inhibiting powder flowing.

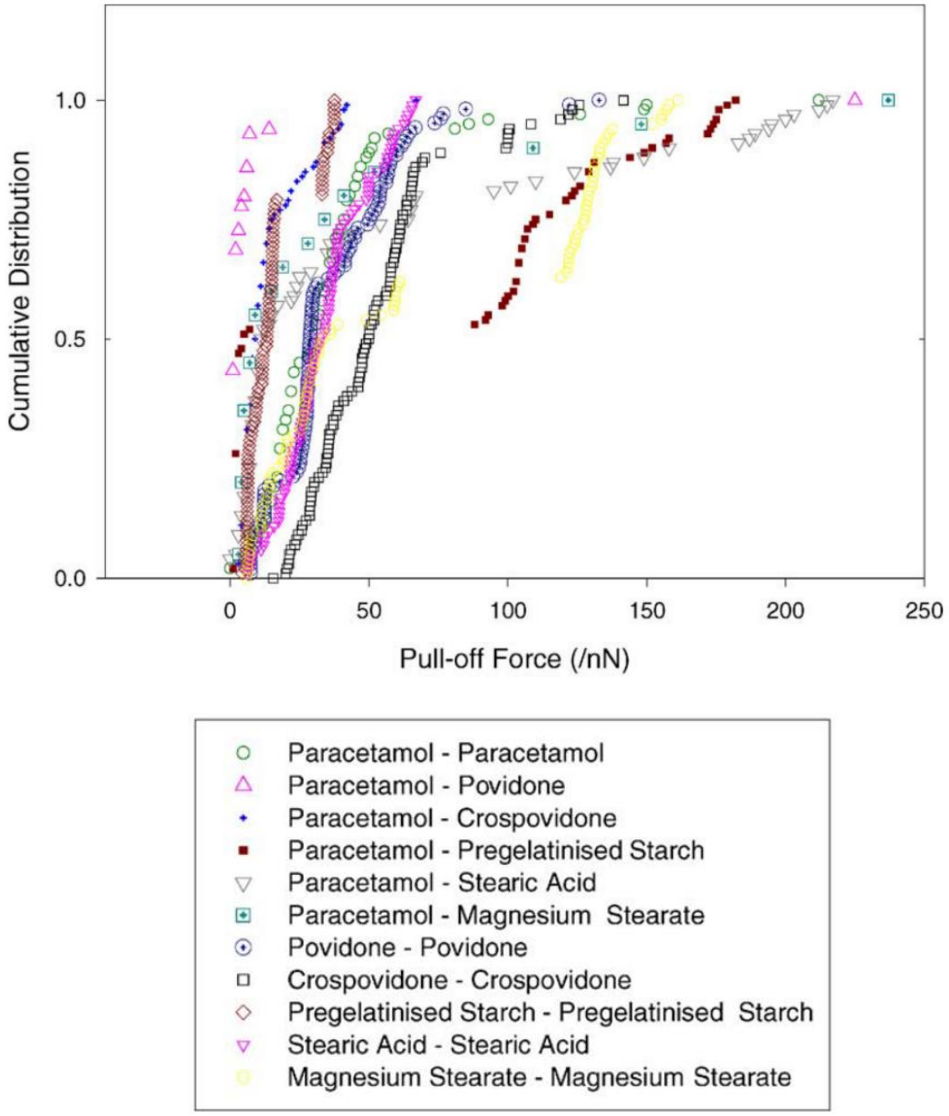

Fig. 2-3 Cumulative distribution of pull-off force for particle-particle interfaces [38]

Besides measuring pull-off force, AFM is also capable of measuring surface roughness of powder particles. Surface roughness of powder particle is an essential property that determines the frictional force between particles, which further impacts bulk powder properties, such as flowability and packing density. There is work that tried to measure the surface roughness of virgin and reused AISI 316L powder particles by AFM [19], as shown in Fig. 2-4. Tapping mode was applied and powder was sprinkled on a drop of silver paint, blowing off excess particles with compressed nitrogen gas. It was found that there is a decrease in surface roughness on particles of reused powder, which might be due to the loss of dendrite exteriors.

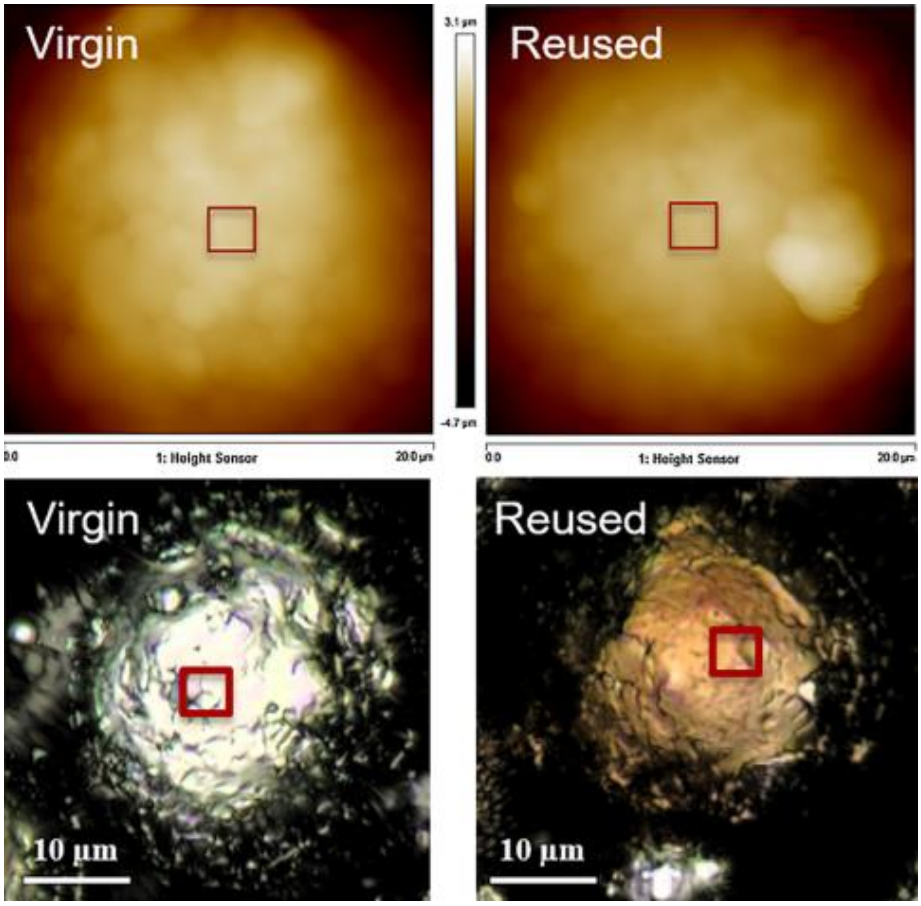

Fig. 2-4 Top: AFM measurement areas for a virgin and reused particle; bottom: confocal microscope images for different virgin and reused particles [19]

Although it is possible to measure the surface roughness of powder particles with AFM, it is extremely time-consuming and challenging to obtain representative data. A technique is still needed that is able to measure the surface roughness of a large number of powder particles within reasonable time.

Much more effort has been devoted to characterizing the impact of recycling powders in PBF processing on the resulting properties and rheological performance. Generally, the basic powder properties, such as particle shape, particle size distribution or chemical composition might change after additive manufacturing process, so the rheological performances of recycled powders might be different from virgin powders [13], [14], [20], [39]. Effect of powder reuse time on Ti-6Al-4V powder characteristics was investigated after the powder was reused for 21 times [39]. The results showed that particle size distribution becomes narrower after reused, which might result from the detachment of fine particles due to the compressed gas flow during powder collection. Also, the reused powder was found to be deformed and less spherical. The oxygen content was found to increase progressively with reuse time, which occurs when the powder is exposed to air. The flow rate of reused powder was unexpectedly higher, which can be explained by the reduction in satellites and moisture content in reused powders.

Similar work has been done by studying the flow characteristics of virgin and recycled Inconel powder [13]. In this case, the particle size distributions of virgin and recycled powders were basically identical, while there was slightly deformation on recycled powder particles, which makes them no longer spherical in shape. Due to the difference in particle shape, recycled powder exhibited considerably lower flowability, as indicated by higher flow energy and lower packing density. Concerning the fact that different powder atomization methods or recycling can

significantly change powder properties, the selection of atomization gas might also impact the characteristics of powders, which has not been sufficiently explored.

The existing work mostly focused on the role of particle size distribution, cohesion and recycling in powder rheology, while there are other basic powder characteristics that might also impact rheological response, such as surface chemistry and internal porosity. Surface chemical composition can be obtained by X-ray photoelectron spectroscopy [19]. Surface chemistry, which is typically slightly different from bulk composition, largely determines the contact potential difference of particle surfaces, which greatly contributes to the charging behavior of powders [40]. Electrostatic force, generated by charging between particles, significantly contributes to cohesive force, which will definitely impact powder flow characteristics and rheological performance. However, powder charging is a complex physical process and the mechanism of it is still unclear, so more work is needed to investigate the role of powder charging in powder rheology. Different from powder charging, the existence of internal porosity is more straightforward [5]. However, since it is usually inside of powder particle and not easy to be detected with traditional powder characterizations, the role of internal porosity in powder rheology is still rarely explored, while it might impact many rheological processes.

2.3 Discrete Element Modeling (DEM) Simulations

Elucidating the flow or spreading of powders is greatly aided by studying the rheology of powder. Although powder rheology can be experimentally studied, only macroscopic information can be obtained, such as avalanche angle and flow energy, which provides little insight on microscopic powder interaction. Discrete element modeling has become the method of choice for researchers and engineers to better understand powder behaviors, which has already been used

over a wide range of applications, including pharmaceutical powders [41], polymers [42], geotechnical applications [43], and also powder rheology [44].

An analysis of dynamic behavior of glass beads subjected to standard FT4 testing was conducted using a combination of experiment and discrete element modeling [45]. Flow energy was calculated through both experiment and simulation based on the measurement of torque and downward force on the blade. The simulation was validated by adjusting the slide friction coefficient between particles, as shown in Fig. 2-5, which indicated that flow energy is greatly dependent on the friction between particle surfaces. The simulation also reported the stresses in front of the blade, which indicates that the shear stress is roughly constant along the blade length.

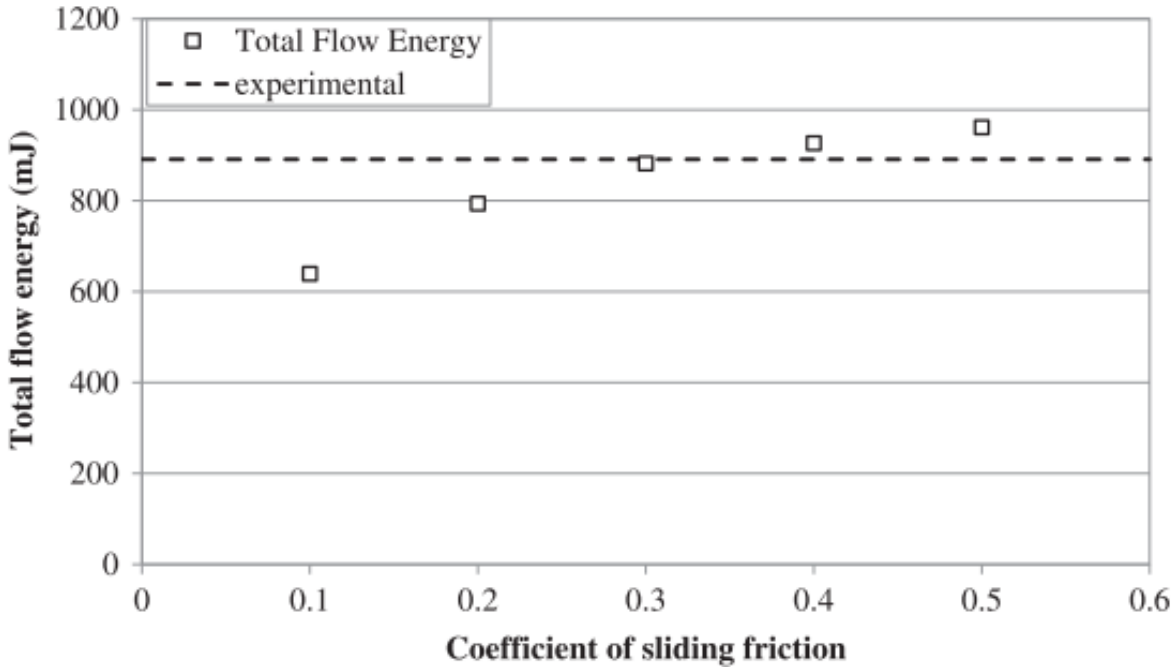

Fig. 2-5 Influence of sliding friction coefficient on flow energy [45]

Particle shape is a crucial property of particle, and it has been shown that particle shape has a great impact on the stress distribution in a sandpile, as indicated by DEM simulations [46]. It has been shown that with aspect ratio deviating from one, the angle of repose increases

significantly and the magnitude of contact force as well. The simulation indicated that non-spherical particles have more pronounced stress dip than spherical particles, as shown in Fig. 2-6, which helps reveal that different morphologies of powder particles result in different particle interactions. Another important characteristic of powder is packing, which was also explored by discrete element modeling simulations [47]. As the same as revealed by experiments, the simulations showed that particle size, particle shape and surface energy all impact packing density. Coordination number of each particle was obtained from simulations to incorporate with packing density measurement, and it was found that the coordination number increases with the increase of packing density. Based on the simulation results, particle size is not the dominant factor that influences packing density. By contrast, aspect ratio and surface energy play more important roles impacting packing density.

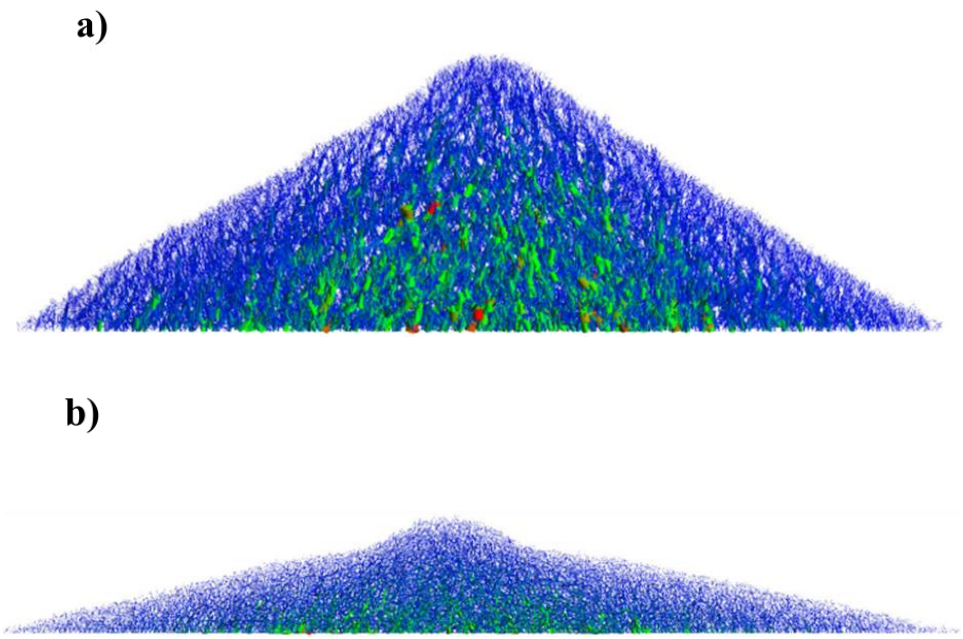

Fig. 2-6 Force network for particle with aspect ratio a) 0.25 and b) 1.0 [46]

Although DEM simulations can provide microscopic information on powder interaction, which helps better understand the physics behind the results of powder characterizations, there are

still limitations that need to be overcome in order to make the most use of it. First, due to the fact that metal powders for additive manufacturing process are typical small (particle size is ~ 100 μm) and hard (Young's modulus is ~ 10^{11} Pa) [44], the simulation timestep is typically extremely small, according to the relation in equation 2-1, which results in huge computational cost. Here, Δt is the timestep of simulation, m_{min} is the smallest mass of particle in the powder, k_n is the stiffness of particles, which is proportional to Young's modulus.

$$\Delta t \sim \sqrt{\frac{m_{min}}{k_n}} \tag{2-1}$$

Second, although there is some work that simulating the interaction of real metal powders for additive manufacturing, there is no standard way that established to measure the variables needed in the simulations, for example, slide or rolling friction, surface energy and morphology for non-spherical powder particles. Currently, calibration of material variables is typically used to obtain reasonable results, while the fact is that different combinations of variables might result in similar simulation results.

Chapter 3

Traditional Powder Characteristics Measurements

In order to evaluate the impact of different atomization gases on the resulting powder properties, three unique lots of AISI grade 316L austenitic stainless-steel powders were sourced from different vendors with the requirement that they be suitable for use in EOS M280 PBF AM system. Two of the lots were atomized using nitrogen (EOS of North America and LPW Technology Limited, UK), and the third was atomized using argon (LPW Technology Limited, UK). Basic powder characteristics were obtained with different powder characterization tools, including chemical composition, particle size distribution and particle morphology. Traditional powder characterizations were also conducted.

3.1 Chemistry

Prior to processing the powder feedstocks, chemical composition was obtained using various techniques at a certified testing laboratory (Westmoreland Mechanical Testing & Research, Inc., in Youngstown, PA) and the results were listed in Table 3-1. The C, S, O, and N concentrations were obtained using a LECO combustion technique as per ASTM E1019-11 [48]. Inductively coupled plasma spectroscopy (ICP), as per ASTM E1479-99 [49], was then used to measure the concentrations of the remaining elements. Based on the values shown in Table 3-1, the concentrations for all of the powders characterized here satisfied the general chemistry requirements for 316L austenitic stainless steel [50]. Since the powders were atomized using either nitrogen or argon atomization gases, additional attention was paid to the nitrogen levels in the different powders. The nitrogen concentration is 0.06 wt.% in nitrogen atomized powder sample1, 0.09 wt.% in nitrogen atomized powder sample2 and 0.01 wt.% in the argon atomized powder.

Table 3-1. Summary of powder chemistries for 316L stainless steel powder feedstocks.

Atomization gas		**Nitrogen**		**Argon**
Elements	**Specification wt. %**	**Sample 1**	**Sample 2**	
Fe	Balance	Balance	Balance	Balance
Cr	16.00-18.00	17.07	16.68	16.25
Ni	10.00-14.00	13.3	11.80	11.45
Mn	2.0 max	1.54	1.34	1.15
Si	0.75 max	0.38	0.73	0.56
Mo	2.00-3.00	2.44	2.56	2.40
C	0.03 max	0.005	0.019	0.009
S	0.03 max	0.004	0.005	0.005
N	0.1 max	0.06	0.09	0.01
P	0.045 max	0.009	0.003	0.005
O	----	0.04	0.05	0.05

3.2 Particle Size Distribution

The particle size distributions of the powders were assessed by both a laser diffraction (Malvern Masersizer 2000) [51] and image analysis (Malvern Morphologi® G3) [18] to obtain reliable measurements. In laser diffraction, the particle size distribution is determined by measuring the intensity of light scattered by a dispersed powder, as a laser beam passes through it. The scattering pattern is then analyzed to obtain the size of particles. Also, image analysis can be employed to measure the particle size distribution in the Malvern Morphologi® G3 system. This system employs compressed gas to spread powder on a slide of glass to ensure the breakdown of

the agglomerates, and then provides quantification of particle size based on the captured optical images. Particle size distributions can be reported based upon the number of particles or on a volume basis. It is important to note this distinction because the most frequently occurring particle size will not necessarily comprise the majority of the sample volume for a given powder, since the volume of a sphere increases exponentially with its diameter. For instance, if half of the particles within a sample on a numerical basis are 1 µm and the other half are 10 µm, 99.9% of the total volume will be occupied by the larger particles. The results of the Malvern Mastersizer 2000 were reported on a volume basis, while the Morphologi® G3 can report both number-based and volume-based distributions. Fig. 3-1 shows the comparison of particle size distribution of the powder samples. As indicated in Table 3-2, the results show reasonable agreement within the two methods.

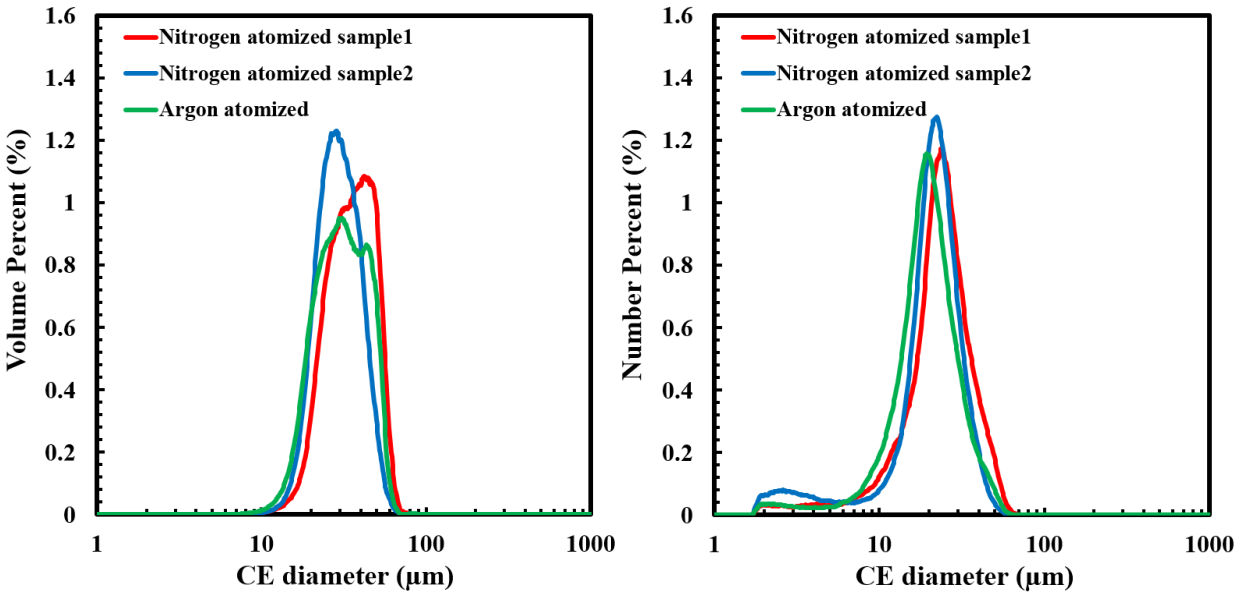

(a) (b)

Fig. 3-1 Circular equivalent (CE) diameter for three powder samples by image analysis

(a) Volume percent and (b) number percent

Table 3-2. Particle size distributions measured using light scattering and image analysis.

Atomization gas		**Nitrogen**		**Argon**
Particle size distribution (μm)		**Sample 1**	**Sample 2**	
Light Scattering				
D10		23.0	19.6	20.1
D50		34.9	29.6	32.4
D90		52.9	44.4	51.3
Image Analysis				
D10	Volume-based	22.2	19.8	18.7
	Number-based	11.8	10.1	10.8
D50	Volume-based	35.1	29.0	30.5
	Number-based	23.4	21.3	19.5
D90	Volume-based	51.4	42.8	48.2
	Number-based	38.0	32.1	31.9

As shown in Fig. 3-1, the particle size distribution for the three powder samples are nearly identical, with nitrogen atomized powder sample1 having slightly larger particle size.

3.3 Morphology

To visualize the powder particles with high resolution, scanning electron microscopy (SEM) was employed. Micrographs of the individual powder particles were obtained, as shown in Fig. 3-2. When examined carefully, it appears that the argon atomized powder has a slightly smoother surface and fewer satellites than the nitrogen atomized powder particles. Overall, there is no obvious difference in the morphology of the samples based on the images.

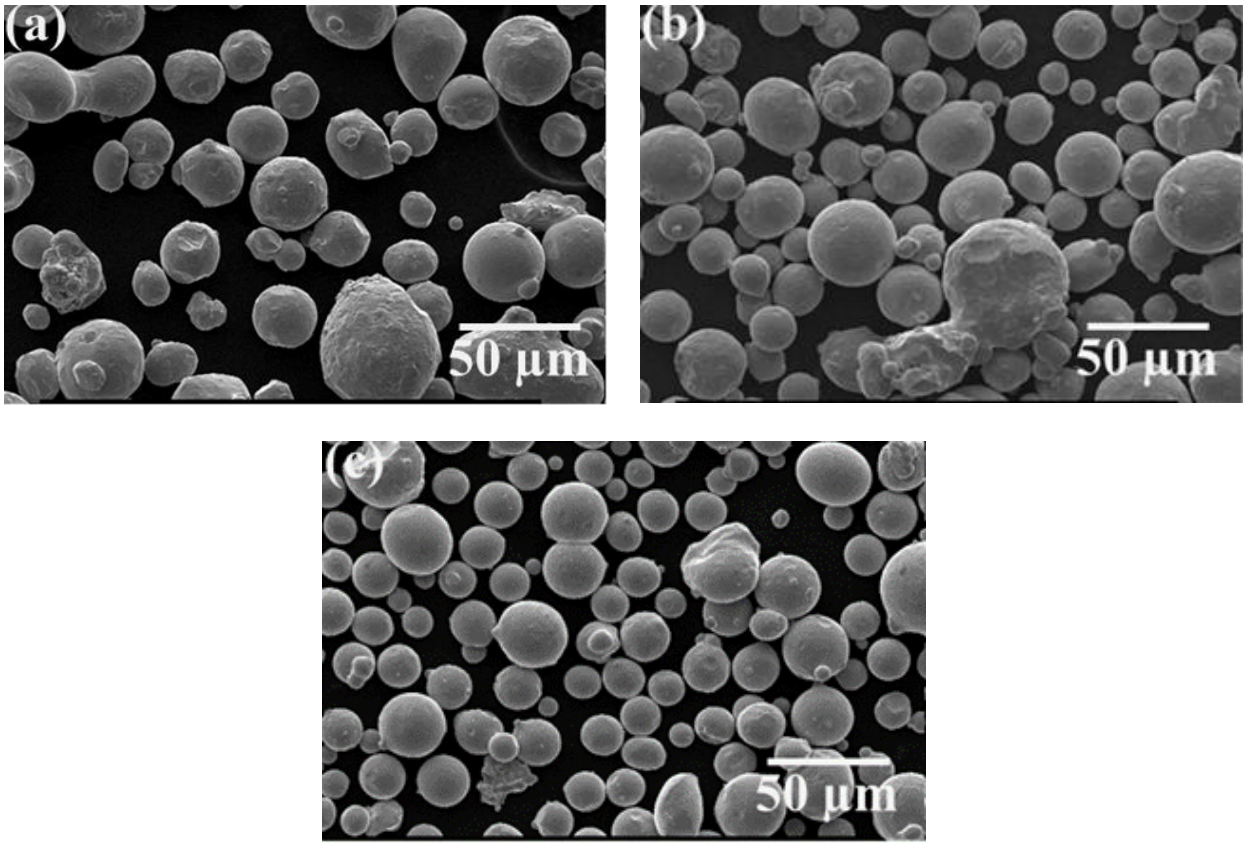

Fig. 3-2. Micrographs showing the particle morphology of (a) nitrogen atomized sample1, (b) nitrogen atomized sample2, and (c) argon atomized powder

3.4 Traditional Powder Characterizations

Each as-received powder feedstock was characterized using a range of conventional powder metallurgy methods for evaluating flowability [24], apparent density [25] and tap density [26]. A standard Hall funnel [24] was used to measure flow rate by the Hall flow test and combined with a 25 cm^3 brass cup [25] to measure apparent density and angle of repose. Average values were calculated from at least three measurements for each powder. An average tap density was also determined from at least three measurements. As per ASTM Standard B527 [26], 100 grams of powder was charged into a 25cm^3 cylinder, and tap density was determined by measuring the

final volume after settling the powder with 3000 taps by a QuantaChrome Dual Autotap model DA-1. Relevant powder characterization tools are shown in Fig. 3-3.

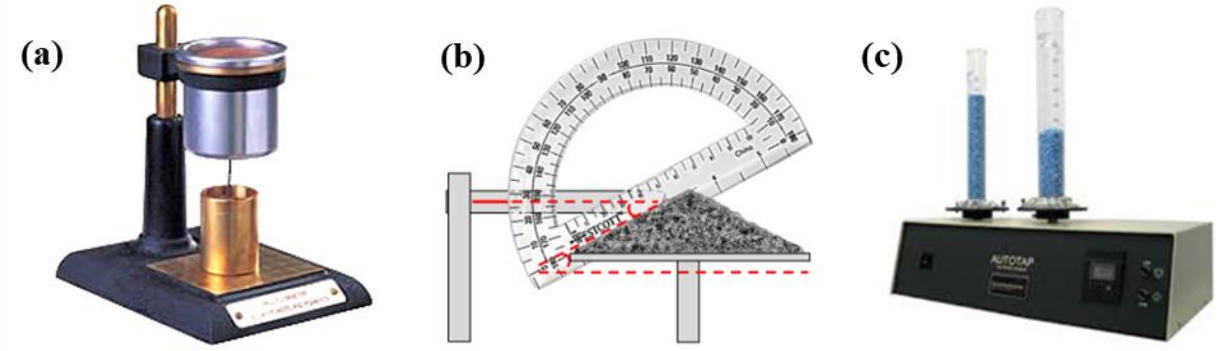

Fig. 3-3 Typical traditional powder characterization tools including

(a) Hall Flowmeter, (b) angle of repose, and (c) tap density

Table 3-3 provides a summary of measurements of these powder properties, including the apparent and tap densities, Hall flow rate and angle of repose. These measurements are typically directed at identifying the packing density and flowability of powder samples. According to the apparent and tap density measurements, argon atomized powder exhibits the highest apparent density and tap density, while nitrogen atomized powders have similarly lower apparent density and tap density compared to argon atomized powder. The ratio of tap density and apparent density is defined as Hausner Ratio (HR), which is considered as an indicator of flowability. The smaller the value, the higher the flowability. The results showed that three powder samples exhibit close HR. Similar to the result of HR, the powder samples exhibit similar flow rate and angle of repose, which means that these traditional flowability tests failed to differentiate the flowability of the powder samples. Modern rheological measurements are needed to further investigate if there is any difference in rheological performance of the powder samples.

Table 3-3. Powder particle measurements made using traditional testing procedures.

Atomization gas	**Nitrogen**		**Argon**
Measurement	**Sample 1**	**Sample 2**	
Apparent Density (g/cm^3)	4.38 ± 0.014	4.35 ± 0.005	4.53 ± 0.014
Tap Density (g/cm^3)	5.00 ± 0.023	5.07 ± 0.014	5.19 ± 0.024
Hausner Ratio	1.14 ± 0.004	1.16 ± 0.002	1.15 ± 0.008
Flow Rate (s/50g)	13.25 ± 0.155	14.27 ± 0.170	13.14 ± 0.100
Angle of Repose (degree)	31.64 ± 0.780	32.64 ± 1.960	30.87 ± 0.870

Chapter 4

Rotating Drum Method

Rotating drum method, used by Revolution Powder Analyzer (RPA), was employed to investigate the rheological performance of the powder samples. The schematic diagrams were shown in Fig. 4-1. This method uses a digital camera to capture the geometry of the avalanche of the powders in the drum, and image analysis is employed to analyze the behaviors of powders during the building, peak, and minimum stages of the avalanche cycle. The rheological measurements were divided into three main categories, including flowability, packing density and shear property, as shown in Table 4-1.

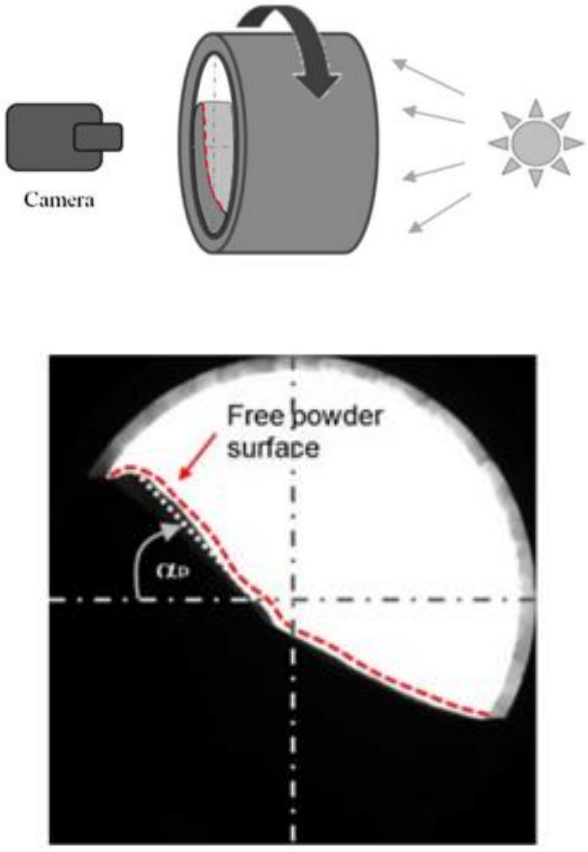

Fig. 4-1 Schematic diagram of the Revolution Powder Analyzer principle [52]

Table 4-1. Rheological measurements made using rotating drum method.

Atomization gas	**Nitrogen**		**Argon**
Powder Rheology Measurements	**Sample 1**	**Sample 2**	
Flow			
Avalanche angle (deg)	40.88 ± 2.160	41.04 ± 2.290	36.65 ± 2.050
Rest angle (deg)	30.32 ± 1.920	31.24 ± 2.380	29.57 ± 1.760
Abs Break energy (mJ/kg)	124.3 ± 4.20	126.6 ± 3.30	121.3 ± 2.10
Rest energy (mJ/kg)	115.7 ± 3.00	117.7 ± 3.70	114.6 ± 2.50
Avalanche energy (mJ/kg)	8.68 ± 0.025	8.77 ± 0.115	6.64 ± 0.205
SL ratio	0.34 ± 0.006	0.33 ± 0.001	0.30 ± 0.001
Packing			
Dynamic density (g/cm^3)	4.26 ± 0.010	4.22 ± 0.020	4.45 ± 0.010
Shear			
Cohesion-T (Pa)	57.57 ± 0.990	62.92 ± 3.550	38.24 ± 1.220
Yield Strength (Pa)	74.25 ± 1.060	74.43 ± 0.720	55.49 ± 1.410

4.1 Flowability

Numerous parameters that indicate flow properties can be provided by RPA, as shown in Table 4-1. Avalanche angle is measured right before the avalanche. Corresponding to avalanche angle, the potential energy of powder right before the avalanche is absolute break energy. It indicates the energy accumulated before an avalanche occurs, and the higher the absolute break energy, the higher the interparticle force. Similarly, rest angle and rest energy are measured right

after an avalanche. They both indicates the energy that is kept in the powder after flowing. During an avalanche, powder flow is inhibited by interparticle forces, and higher interparticle forces would more readily inhibit powder flow, so higher rest angle and rest energy result from higher interparticle forces. Avalanche energy is the potential energy difference before and after an avalanche, which can be interpreted as the energy needed for certain amount of powder to flow. Higher avalanche energy indicates a higher level of interparticle force. Powder can act as a solid, because it is able to form a certain shape. At the same time, it can also act as a liquid when it is flowing. SL ratio describes how much the powder acts as a solid versus as a liquid. Lower SL ratio indicates the powder acts more like a liquid, which flows better. Surface fractal provides an indication of how rough the powder surface is during the avalanche process [53]. If the surface is rough and jagged, the surface fractal will be greater than one, ranging from 2 to 11, depending on how rough the surface is. The surface fractal of the powder samples was shown in Fig. 4-2. The results showed that surface fractal of the three powder samples are similar.

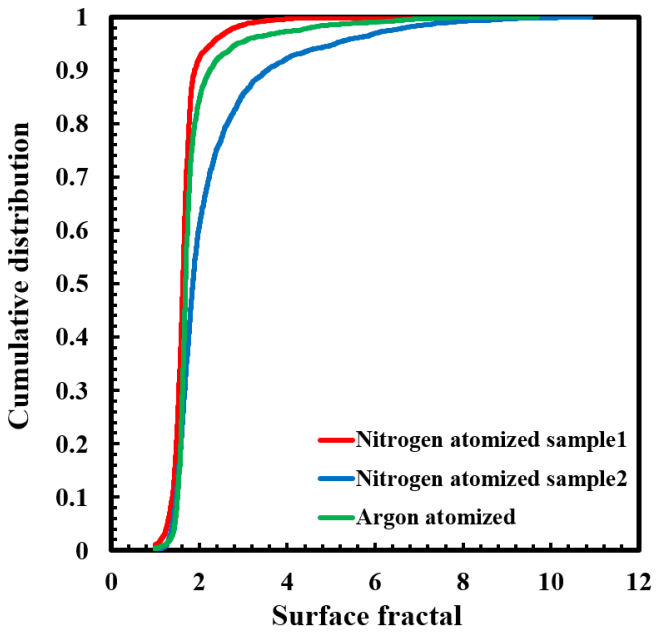

Fig. 4-2 Cumulative distribution of surface fractal of each powder sample

As shown in Table 4-1, the flowability results obtained from RPA are pretty consistent, with argon atomized powder exhibiting the lowest avalanche angle, rest angle, absolute break energy, rest energy, avalanche energy and SL ratio, since they are from the same physical process. Among these parameters, avalanche angle is the most generally reported one. With higher avalanche angle, higher gravity force is needed for an avalanche to occur, correlating higher interparticle force and lower flowability. As shown in Fig. 4-3, nitrogen atomized powders exhibit similar avalanche angle, which is around 5 degrees higher compared to argon atomized powder. To understand the difference in flowability, a correlation to basic powder characteristics is needed. As shown in chapter 3, the particle size distributions of the powder samples are nearly identical as well as the morphology based on SEM images. However, observation is not always an effective way to distinguish different morphologies of powder particle.

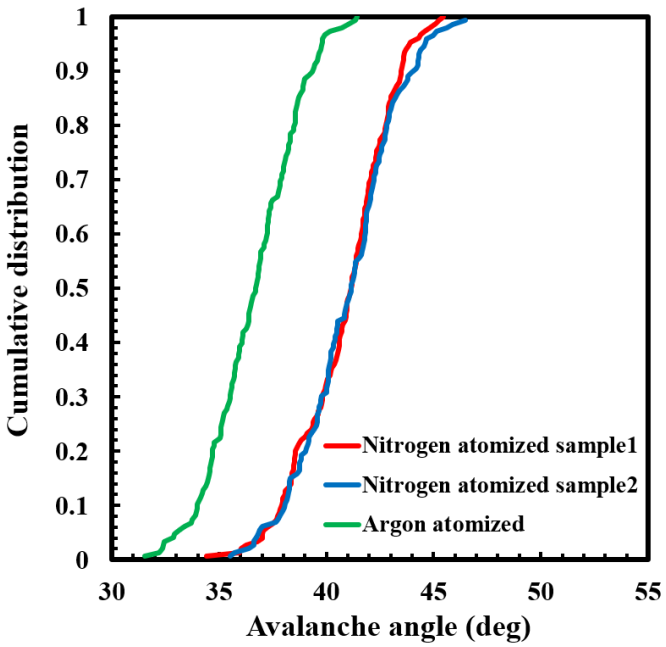

Fig. 4-3 Cumulative distribution of avalanche angle of each powder sample

A more in-depth study of the particle morphologies of the powder samples can be made using more modern image analysis tool, Morphologi® G3. This tool can provide information concerning the convexity, aspect ratio, and circularity of powder particles, as shown in Table 4-2. Convexity, a measure of the surface roughness, is calculated by dividing the convex hull perimeter by the actual particle perimeter; a perfectly smooth surface has a convexity value of unity as more jagged surfaces will deviate further below unity. Aspect ratio relates the measured width to length of the individual particles. For a perfect sphere, the aspect ratio has a value of unity. Circularity provides information on both surface roughness as well as particle shape. A perfectly circular particle has a circularity value of unity, and any deviation from a perfect circle in either surface roughness or shape will result in a lower circularity value. The values shown in Table 4-2 are the number-based distribution values of all the particles in each powder sample. The number of particles that measured was 84338 for nitrogen atomized powder sample1, 130967 for nitrogen atomized powder sample2 and 159953 for argon atomized powder, and the large numbers of particles were to ensure the samples are representative. The number-based frequency of values for these morphology parameters, calculated from measurement of every particle in each powder sample, were shown in Fig. 4-4(a) for convexity, Fig. 4-4(b) for aspect ratio, and Fig. 4-4(c) for circularity. As shown in Fig. 3-3, the particle morphology parameters of the three powders are similar. However, if examined closer, there is a small difference in aspect ratio, with argon atomized powder having a higher fraction of particles with higher aspect ratio. Assuming aspect ratio of 0.9 to 1 as highly spherical, after adding all the frequency values in this range, it turned out that argon atomized powder has around 65 percent particles that are highly spherical, while there are 55 percent particles in nitrogen atomized powders are highly spherical. This indicates

that argon atomized powder has 10% more highly spherical particles compared with nitrogen atomized powders

Table 4-2. Summary of particle morphology measurements.

Atomization gas		**Nitrogen**		**Argon**
Particle Morphology Parameters		**Sample 1**	**Sample 2**	
Number of particles in sample		84338	130967	159953
Convexity	D(N, 10)	0.962	0.966	0.966
	D(N, 50)	0.992	0.992	0.993
	D(N, 90)	0.998	0.999	0.999
Aspect Ratio	D(N, 10)	0.701	0.717	0.743
	D(N, 50)	0.911	0.914	0.94
	D(N, 90)	0.982	0.984	0.989
Circularity	D(N, 10)	0.899	0.912	0.912
	D(N, 50)	0.978	0.978	0.983
	D(N, 90)	0.994	0.995	0.996

More obvious difference can be identified from cumulative distribution, as shown in Fig. 4-5. It indicates that argon atomized powder has 10% more particles with aspect ratio of 0.9 to 1, which is assumed as highly spherical. This difference in particle morphology might result from the different atomization gases. Argon has a lower thermal conductivity than nitrogen over a wide temperature range. For example, within 1000K to 2000K, the thermal conductivity of argon is 50 ~ 75 mW*m-1*K-1, while the thermal conductivity of nitrogen is 70 ~ 100 mW*m-1*K-1 [54].

With lower thermal conductivity, the cooling rates through the liquid and solid/liquid regions are slowed during atomization process, allowing the molten metal droplets to cool more slowly and for the particle shape to transit to a spherical shape.

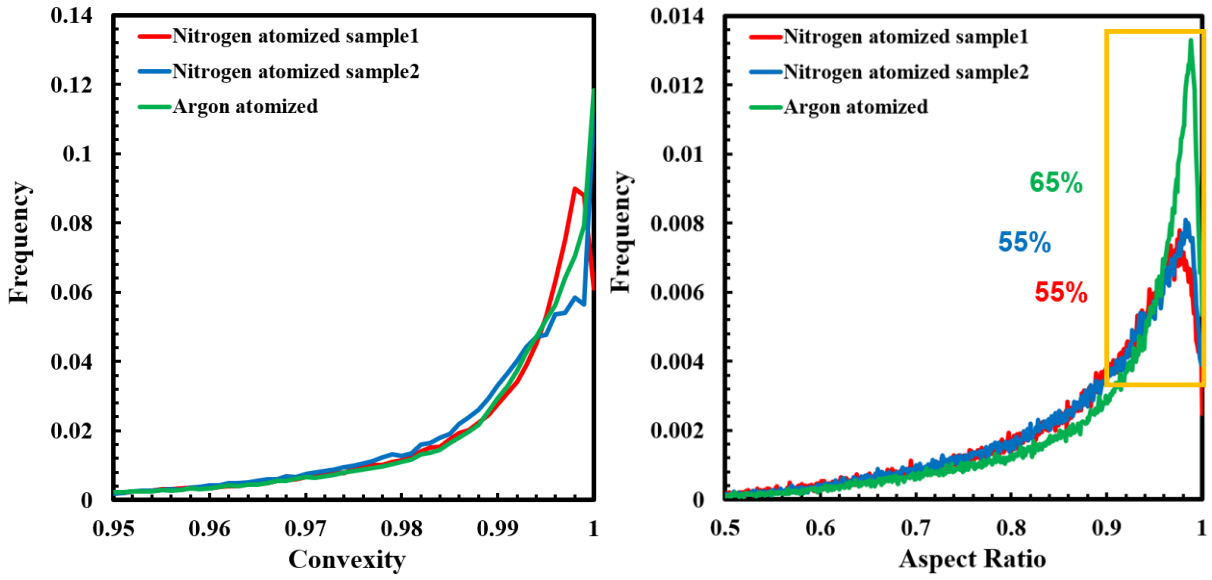

(a)

(b)

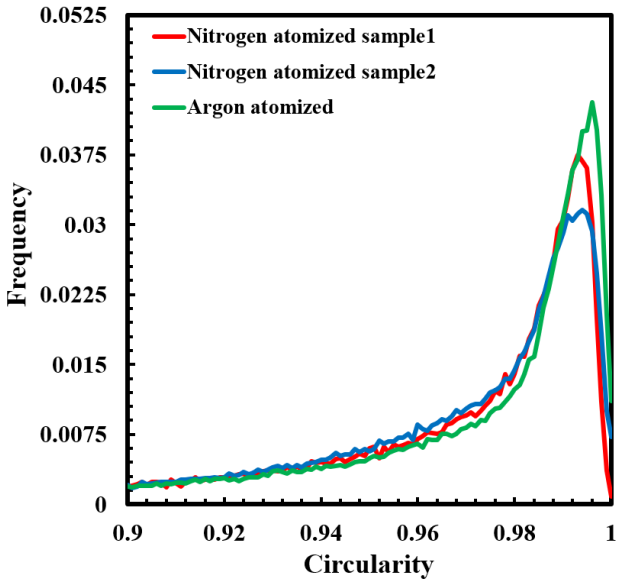

(c)

Fig. 4-4. Morphology of particles in each powder sample

(a) Convexity, (b) aspect ratio, and (c) circularity

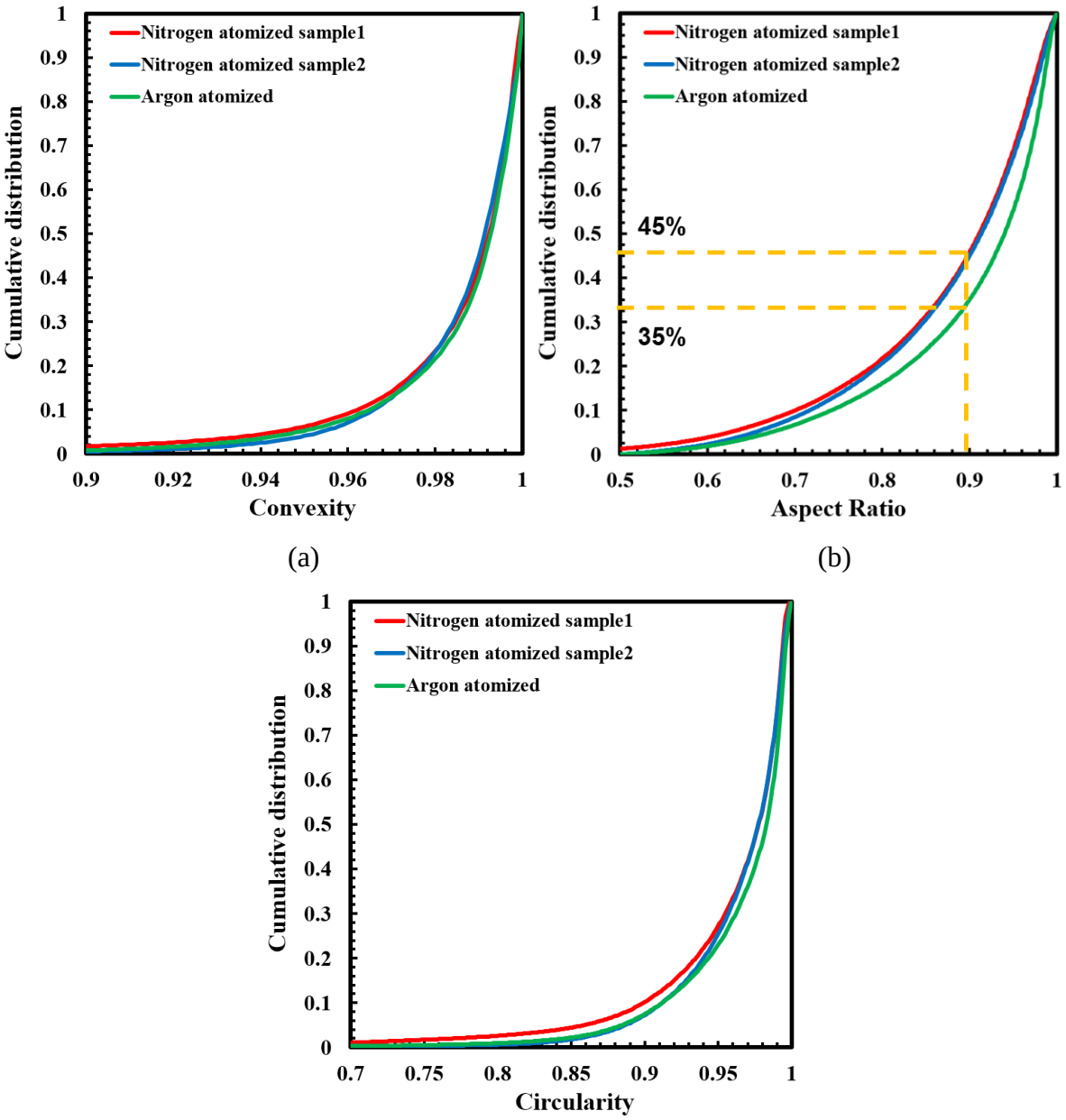

Fig. 4-5. Cumulative distribution of morphology parameters for each powder sample (a) convexity, (b) aspect ratio, and (c) circularity

Interestingly, there is strong correlation between particle size and particle morphology in each of the powder samples. Particle size, roughly between number-based D10 and D90, was divided into five ranges, and cumulative distribution was calculated for morphology parameters of

each powder sample. The results showed that larger particles tend to be less spherical, as indicated in Fig. 4-6.

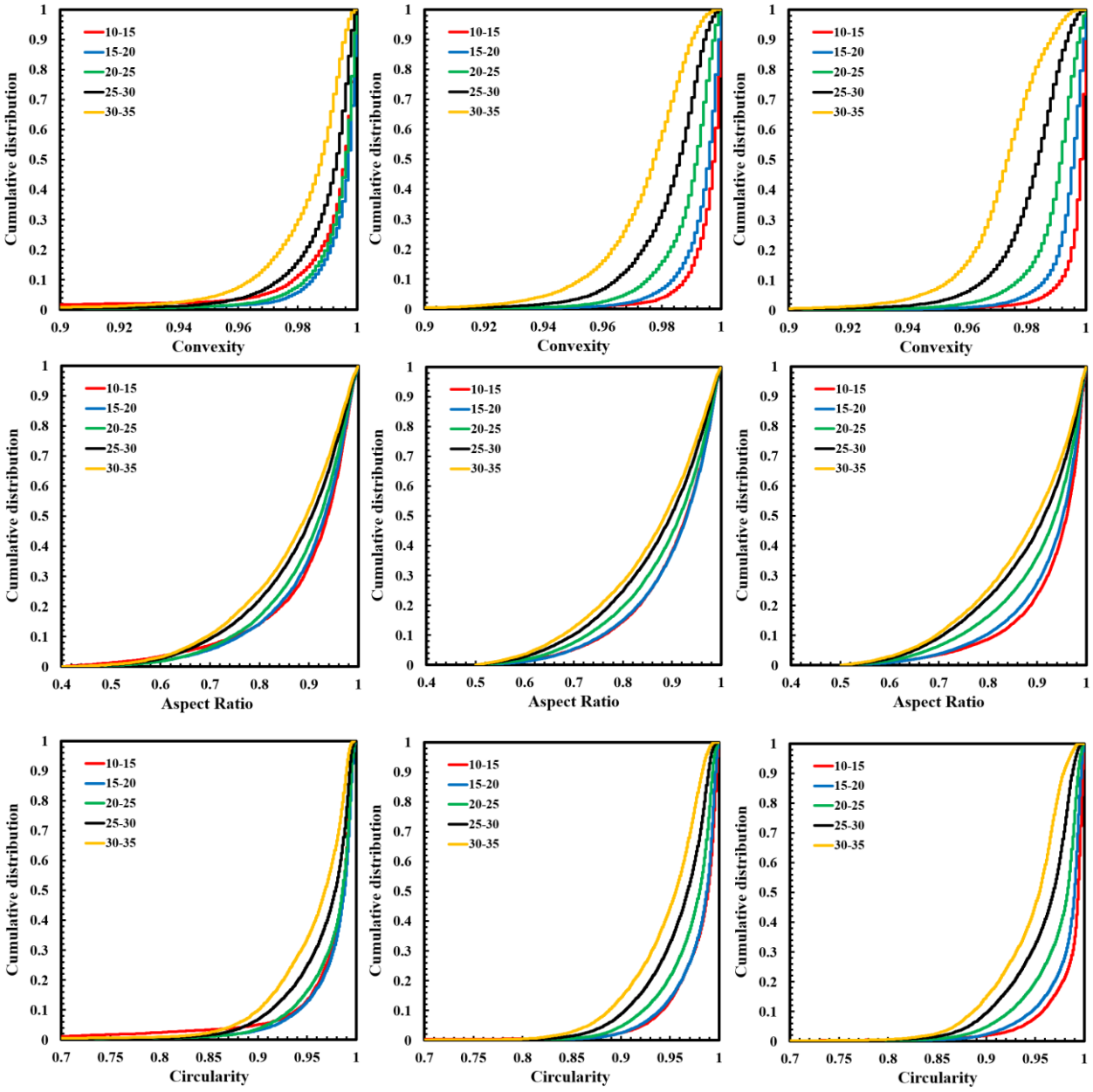

Fig. 4-6. Morphology of particles of different sizes in each powder sample

(a) Nitrogen atomized sample1, (b) nitrogen atomized sample2, and (c) argon atomized powder

Overall, there is a correlation between aspect ratio of powder particles and flowability of the powder. Argon atomized powder has 10 percent more highly spherical particles as reflected by aspect ratio, and at the same time, argon atomized powder exhibits higher flowability compared with nitrogen atomized powders as indicated by 5 degrees lower avalanche angle. To further investigate the impact of aspect ratio on particle interaction, discrete element modeling (DEM) simulations of particle behaviors in a rotating drum were conducted on the open-source LIGGGHTS particle simulation software [55].

4.2 Discrete Element Modeling Simulations

DEM was firstly developed by Cundall and Strack, and the concept of it is to treat every particle, such as grain of sand, powder particle or rock particle, as individual, which will interact with other particles within a specific distance. Newton's laws of motion are used in DEM simulations for conservation of momentum and angular momentum [56]. In idealized particulate DEM, contact forces between two particles are usually determined by introducing "virtual springs" at the contact points [57]. In this work, a linear spring-dashpot model was employed to predict the motion of particles, as shown in Fig. 4-7, which is known as "gran model hooke" in LIGGGHTS [55]. This model requires material properties, such as Young's modulus, Poisson's ratio, coefficient of friction and coefficient of restitution, to calculate contact forces with following formulas:

$$F_n = k_n \Delta x_n - \gamma_n \Delta v_n \tag{4-1}$$

$$F_t = -k_t \Delta x_t - \gamma_t \Delta v_t \tag{4-2}$$

Where F_n is the normal force between contacting particles, k_n is the normal spring stiffness, γ_n is the viscoelastic damping constant for normal contact, Δx_n is the overlap distance of particles and

Δv_n is the relative velocity between particles in normal direction. Similarly, in tangential direction, F_t is the force between contacting particles, which fulfils $F_t \leq \mu_s F_n$, μ_s is the coefficient of static friction, k_t is the spring stiffness, γ_t is the viscoelastic damping constant, Δx_t is the overlap distance of particles and Δv_t is the relative velocity between particles. The elastic spring stiffness and viscoelastic damping constant could be determined by:

$$k_n = k_t = \frac{16}{15}\sqrt{R^*}Y^*\left(\frac{15m^*v^2}{16\sqrt{R^*Y^*}}\right)^{1/5} \tag{4-3}$$

$$\gamma_n = \gamma_t = \sqrt{\frac{4m^*k_n}{1+\left(\frac{\pi}{\ln(e)}\right)^2}} \tag{4-4}$$

Where v is characteristic impact velocity, which is the velocity of particle before collision, $1/R^* = 1/R_1 + 1/R_2$, $1/m^* = 1/m_1 + 1/m_2$, $1/Y^* = (1 - v_1^2)/Y_1 + (1 - v_2^2)/Y_2$. Y, e, R and m are the Young's modulus, coefficient of restitution, radius and mass of the particle, respectively. Besides static friction, rolling friction (μ_r) is also implemented using the elastic-plastic spring dashpot (EPSD2) model with an additional torque contribution. Details regarding the model can be found in the LIGGGHTS online documentation and in [58]. For the stability of simulation, the critical time step needs to be determined. Generally, the critical time step can be estimated based on the relation:

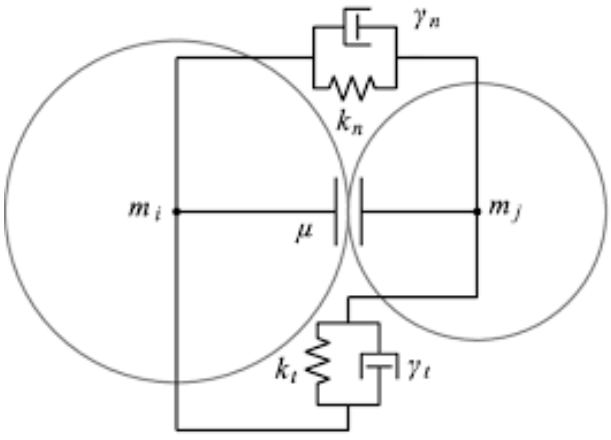

Fig. 4-7 Schematic diagram of contact model of particles [57]

$$\Delta t \sim \sqrt{\frac{m_{min}}{k_n}} \tag{4-5}$$

Where m_{min} is the minimal mass of particles, and k_n is the stiffness of the material. The critical time step can be checked by comparing it with Rayleigh time and Hertz time to ensure the stability of simulations [55].

4.2.1 Experimental Validation

Rotating drum method was used for experimental validation by employing the Revolution Powder Analyzer (RPA). Stainless-steel beads in different sizes, with the bulk volume of 100ml, were charged into a drum made of aluminum with glass sides. Although the particles flow very well, there is still an avalanche behavior, so that avalanche angle, avalanche energy and many other parameters can be measured. A "drum", with the same size of that in RPA, was generated with SolidWorks for the simulation. The same weight and size of particles in the experiment were generated in the "drum", and a rpm of 1 was used in both experiment and simulation. To determine the parameters for the simulation that are able to replicate the experiment, a range of coefficients of static friction and rolling frication were used and compared with experimental results. Table 4-3 lists the values of the parameters in the simulation that are validated by the experiment, as shown by avalanche angle in Fig. 4-8 and potential energy in Fig. 4-9. Among the material properties, general values of density and Poisson's ratio for stainless-steel were used, while a reduced Young's modulus was used in the simulations. It has been shown that reducing the Young's modulus from 200 GPa to 200MPa did not significantly affect the angle of repose of powder, while it reduced the computational cost by 62% [59]. Indeed, according to Equation 4-5, a reduction in stiffness, which is dependent on Young's Modulus, leads to a larger timestep and reduces the computational cost.

Table 4-3 Key parameters used in simulation that are validated by experiments

Parameters	Values
Particle size in diameter (mm)	4.8 (90 vol.%) and 2 (10 vol.%)
Particle density (g/cm^3)	7.8
Particle Young's Modulus (MPa)	100
Particle Poisson's ratio	0.3
Particle-Particle/Wall coefficient of restitution	0.5
Particle-Particle coefficient of static friction	0.12
Particle-Wall coefficient of static friction	0.5
Particle-Particle coefficient of rolling friction	1.2
Particle- Wall coefficient of rolling friction	1.8
Timestep (s)	0.000003

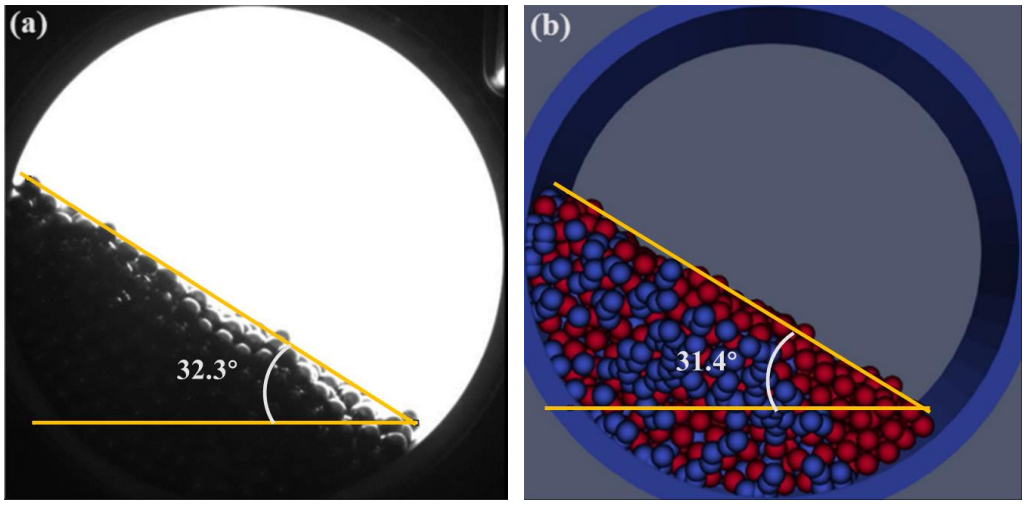

Fig. 4-8 A comparison of avalanche angle from (a) experiment and (b) simulation

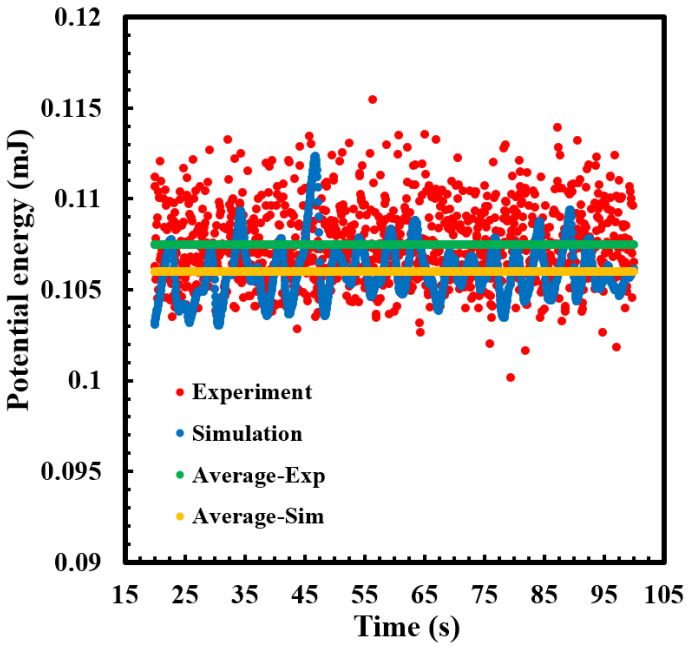

Fig. 4-9 A comparison of potential energy of experiment and simulation

4.2.2 Impact of Aspect Ratio on Particle Interaction

To investigate the impact of aspect ratio on particle interaction, multi-sphere method was employed to generate particles with different aspect ratios for the simulations [55]. In this method, the total force and torque at the center of mass of each multi-sphere particle is calculated by adding up each contact force of its constituent spheres rather than integrate the Newton's laws of motion for each particle [60]. Multi-sphere particles were generated by combining two particles with diameter of 4.8mm, as indicated in Fig. 4-10. The same values of parameters, as listed in Table 4-3, were used to simulate the behavior of particles with different aspect ratios in a rotating drum. The mass of particles used is the same for each simulation, and the number of particles in the simulations is 1040 for aspect ratio of 0.7, 1218 for aspect ratio of 0.8 and 1414 for aspect ratio of 0.9. Avalanche angle was measured with ImageJ. Potential energy and average stress of the particles were provided in the simulation results, and then a comparison was made based on these parameters for each simulation.

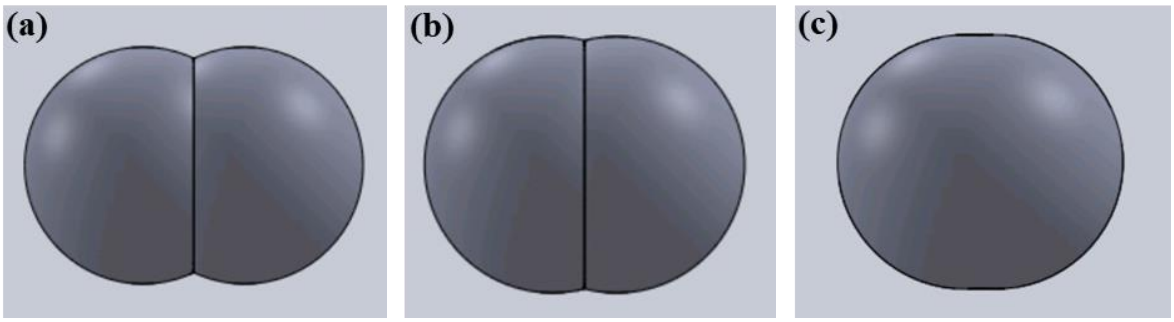

Fig. 4-10 Schematic diagram of particles with different aspect ratios of (a) 0.7, (b) 0.8, and (c) 0.9

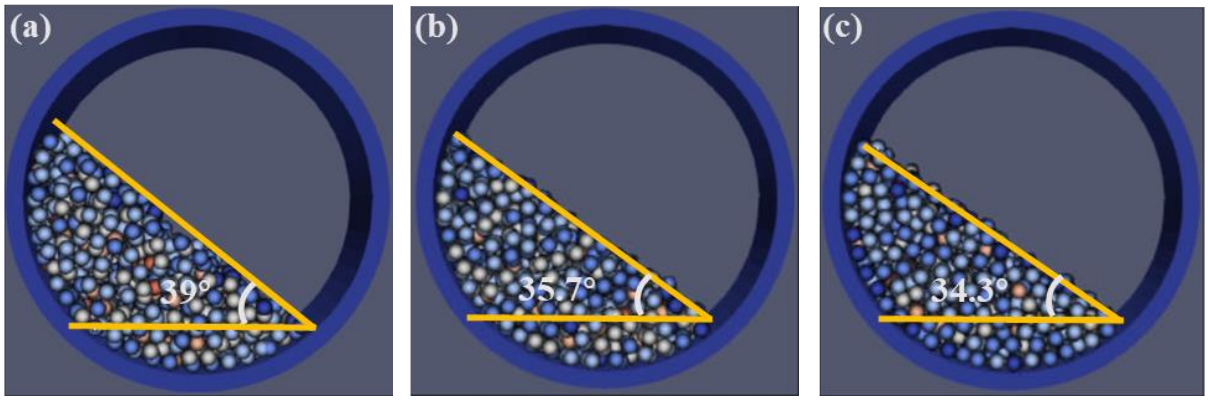

Fig. 4-11 A comparison of avalanche angle of particles with different aspect ratios of (a) 0.7, (b) 0.8, and (c) 0.9

As shown in Fig. 4-11, particles with different aspect ratios exhibit different avalanche angles. Corresponding to this, the evolution of potential energy also appears different, which can be correlated to the small change in aspect ratio, as shown in Fig. 4-12. It seems that particles with lower aspect ratio exhibit higher avalanche angle and absolute break energy. As discussed in Chapter 4, higher avalanche angle and absolute break energy, which can be derived from the evolution of potential energy, indicate higher level of interparticle force. To demonstrate this, it is critical to investigate if small change in aspect ratio can impact the interparticle force, so average

stress of the particles in each simulation was extracted from results, as shown in Fig. 4-13. It clearly shows that the evolution of average stress of the particles is roughly consistent along with time, and particles with lower aspect ratio show considerably higher levels of stress.

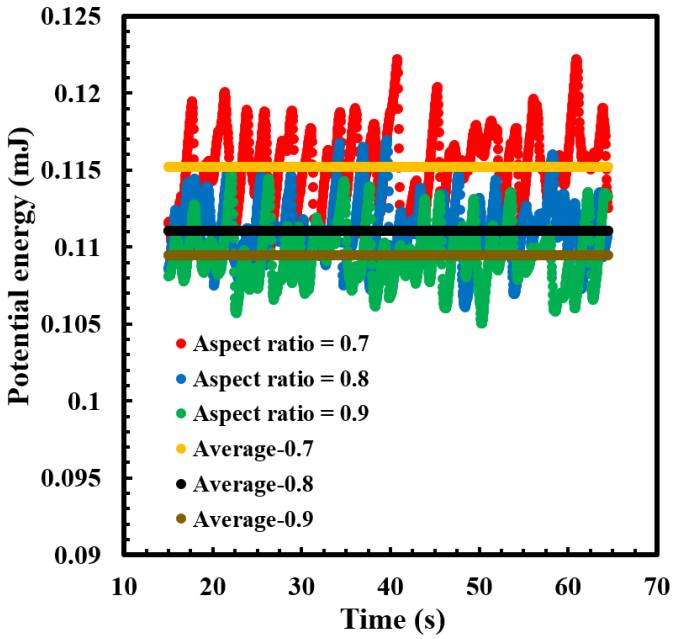

Fig. 4-12 Evolution of the potential energy of particles with different aspect ratio

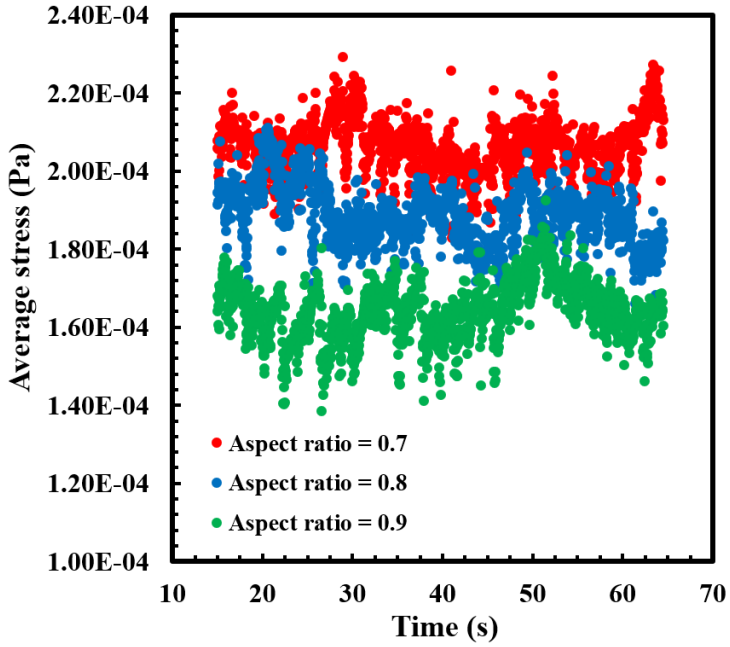

Fig. 4-13 Evolution of the average stress on particles with different aspect ratios

The results indicated that with lower aspect ratio, there is higher level of stress on the particle when it is interacting with other particles, which means a higher level of interparticle force. As discussed before, flowability, packing density and rheological performance are largely dependent on the interparticle force. The simulation results demonstrated that a small change in aspect ratio can impact particle interactions, with lower aspect ratio resulting in higher level of interparticle force, and can further impact rheological responses.

Based on the simulation results, the difference in flowability can be correlated to the different morphology of nitrogen and argon atomized powders. When powder is flowing, spherical particles with aspect ratio of one require the same volume as its own volume to rotate, while particles with low aspect ratio require more space than its own volume to rotate. The lower the aspect ratio, the more space the particles need to rotate, which increases the interactions with surrounding particles and further increases interparticle forces [46]. The results in Table 4-1 indicate that argon atomized powder showed higher flowability than nitrogen atomized powders, which can be correlated to the more spherical particles in argon atomized powder.

4.3 Packing Density and Shear Property

Dynamic density indicates the packing density under dynamic rotating processes. In this dynamic rotating process, particles have high kinetic energy, and more space is needed for the motion of each particle, so dynamic density is generally lower than apparent density. The results of dynamic density match well with the trend of apparent density and tap density. Argon atomized powder exhibits the highest packing density. By comparison, the nitrogen atomized powders have similarly lower packing density.

Cohesion-T is the shear stress that needs to be overcome for certain amount of powder to flow over the powder that does not flow during an avalanche. Yield strength is the shear stress that needs to be overcome to release certain amount of powder before an avalanche. The main difference between cohesion-T and yield strength is that cohesion-T indicates the flow resistance during powder is flowing, while yield strength describes the flow resistance to initiate powder flowing. As shown in Table 4-1, cohesion-T is smaller than yield strength, which means that the flow resistance is lower when powder is flowing. Since cohesion-T and yield strength were measured based on the same physical processes as the measurement of avalanche energy and avalanche angle, the results are consistent with them.

Chapter 5 Powder Rheometer and Shear Cell

Powder rheometer and shear cell, both from FT4 technology, were also employed to investigate the rheological performance of the powder samples. The schematic diagrams were shown in Fig. 5-1 and Fig. 5-2. In powder rheometer, the force and torque on the blade will be measured when the blade is moving in the powder bed. Flow energy will be calculated based on the measured force and torque values. Shear cell measures the shear stress needed to initiate the powder flow. The rheological measurements were divided into three main categories, including flowability, packing density and shear property, as shown in Table 5-1.

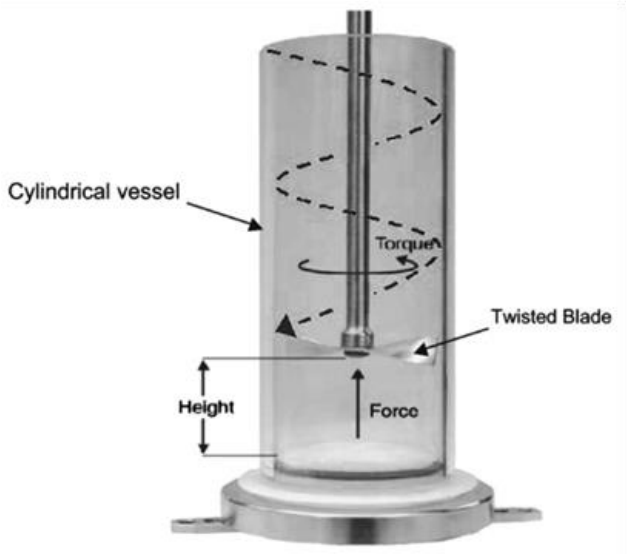

Fig. 5-1 Schematic diagram of the FT4 Powder Rheometer principle [36]

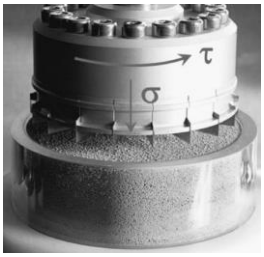

Fig. 5-2 Schematic diagram of the shear cell principle [36]

Table 5-1. Rheological measurements made using FT4 powder rheometer and shear cell.

Atomization gas	**Nitrogen**		**Argon**
Powder Rheology Measurements	**Sample 1**	**Sample 2**	
Flow			
Basic flow energy (mJ)	821.5 ± 32.60	903.5±24.30	861.1±16.80
Specific energy (mJ/g)	2.76 ± 0.090	3.10 ± 0.010	2.68 ± 0.010
Packing			
Conditioned Bulk density (g/cm^3)	4.62 ± 0.010	4.69 ± 0.070	4.88 ± 0.010
Shear			
Cohesion (kPa)	0.13 ± 0.010	0.19 ± 0.001	0.16 ± 0.010
UYS (kPa)	0.38 ± 0.010	0.54 ± 0.005	0.48 ± 0.040
MPS (kPa)	7.94 ± 0.042	7.86 ± 0.058	7.79 ± 0.100
AIF (deg)	21.1 ± 0.56	20.6 ± 0.35	20.9 ± 0.74

5.1 Flowability

Basic flow energy (BFE) is derived by calculating the energy needed for the blade to downwards pass through a powder bed with anti-clockwise rotating under relatively high stress condition, as indicated in equation (5-1), where R is the radius of impeller, α is the helix angle, H is the penetration depth, F is the vertical force and T is the torque acting on the impeller. Different from BFE, specific energy (SE) is derived by moving the blade upwards with clockwise rotating under relatively low stress condition, and the energy is normalized with mass [11]. It is generally accepted that the lower the flow energy, the better the flowability. As shown in Table 5-1, nitrogen

atomized powder sample 2 exhibits the highest BFE, while nitrogen atomized powder sample1 exhibits evidently lower BFE than the other two powder samples, which is different from the results of flowability obtained from RPA. As for SE, nitrogen atomized powders exhibit slightly higher flow energy than argon atomized powder, which roughly follows the avalanche measurements. To understand the unexpected BFE results, the force and torque in one of the tests were shown in Fig. 5-3. Similar results were obtained for other tests. As shown in Fig. 5-3, the absolute values of force and torque on the blade increase as the blade travels downwards into the powder bed, that is because more and more powder would contribute to the flow resistance. Nitrogen atomized powder sample1 requires the lowest force and torque when moved by the blade, which further results in the lowest BFE.

$$E_{flow} = \int_0^H \left(\frac{T}{R\tan\alpha} + F\right) dH, \tag{5-1}$$

Considering the physical process that derives the flow energy when the powder particles were moved by a blade, the force required to move the particles was determined by interparticle resistance, and also the weight of powders. Previous work showed that flow energy can be drastically different among materials with different densities, for example, 1032 mJ for Inconel powders and 150 mJ for aluminum alloy powders [13]. In this case, the three powder samples are all 316L austenitic stainless-steel powders, as shown in Table 3-1, which means they have roughly the same density. True volume of powder, which has not been sufficiently addressed, also determines the weight of the powder. Currently, only bulk volume of powder is considered when deriving flow energy. However, if packing densities of powders are drastically different, the true volume of powders in the vessel might be considerably different, so that the flow energy calculated might not be a pure indication of flowability, but also influenced by the weight of powder. In this case, flowability and packing density of nitrogen atomized powders were roughly the same, while

there was still around 10% unexpected difference in flow energy, which means packing might not be a dominant factor here. Concerning this, another factor that alters the true volume of powder is internal porosity of powder particles, which was identified with µCT and analyzed with Avizo.

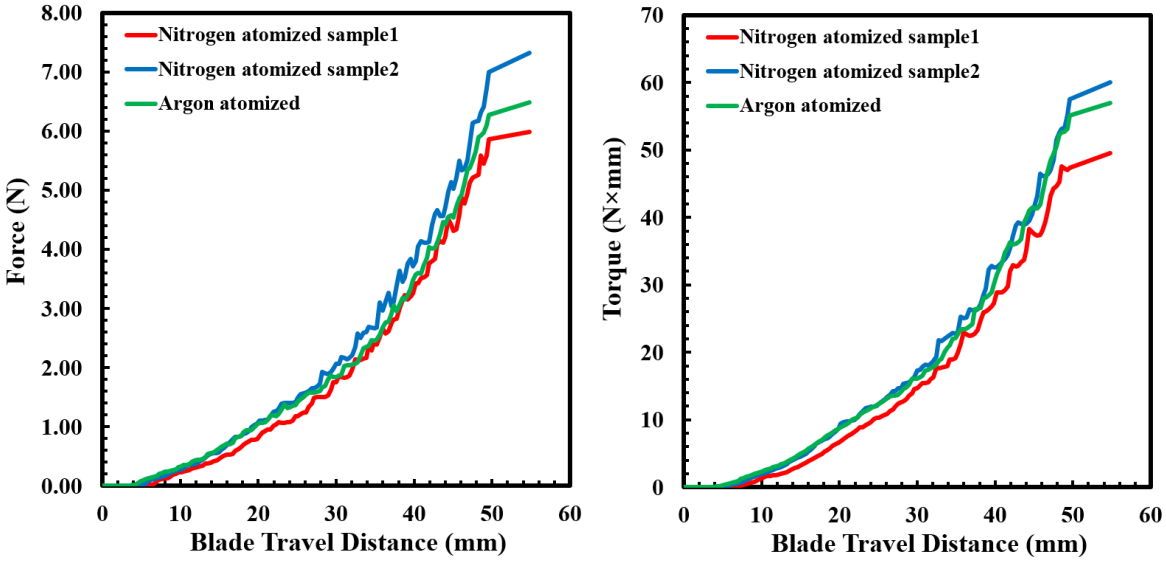

(a) (b)

Fig. 5-3. Force (a) and Torque (b) on the blade in dynamic downwards testing

5.2 Internal Porosity

Micro-computed x-ray tomography (µCT) was used to identify internal porosity of powder particles. Powder samples were filled in 3mm diameter, 3mm tall plastic tubes and the scanning was performed on GE v|tome|x L300 system at 150kV and 30µA with a 0.2mm Al filter. The voxel size was around 1.5µm. The raw data was converted into approximately 2000 cross-sectional images of representative powder samples and stacked together to form image sequences using imageJ Fiji, which is an open source image-processing platform [61]. Visualization of 3D images, material segmentation and internal porosity identification were performed using Avizo 9.7.0. The instruction manual of Avizo could be found here [62]. Fig. 5-4 showed the visualization of internal porosity in some of the particles.

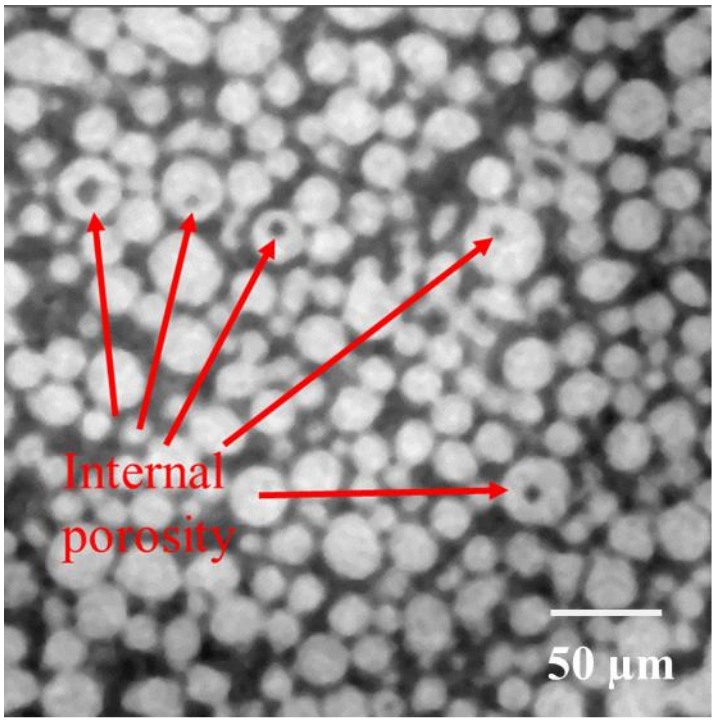

Fig. 5-4 The visualization of internal porosity in powder particles

As indicated in Fig. 5-5, the image sequence was firstly stacked together into a cylinder with imageJ Fiji, and then a cubic region was extracted from the cylinder with Avizo. A 1.2mm×1.2mm×1.2mm cubic region was extracted from each powder sample at the same location for comparison. A smooth step was then conducted to present a clear image with higher contrast. Material segmentation was performed to separate powder particles and pore space based on their intensities with Avizo, and then the isolated pores, which are internal porosities of particles, were highlighted. Fig. 5-6 showed a comparison of internal porosity of powder samples. Based on the images, it seems that nitrogen atomized powder sample1 has considerably more internal porosities compared to nitrogen atomized powder sample2 and argon atomized powder.

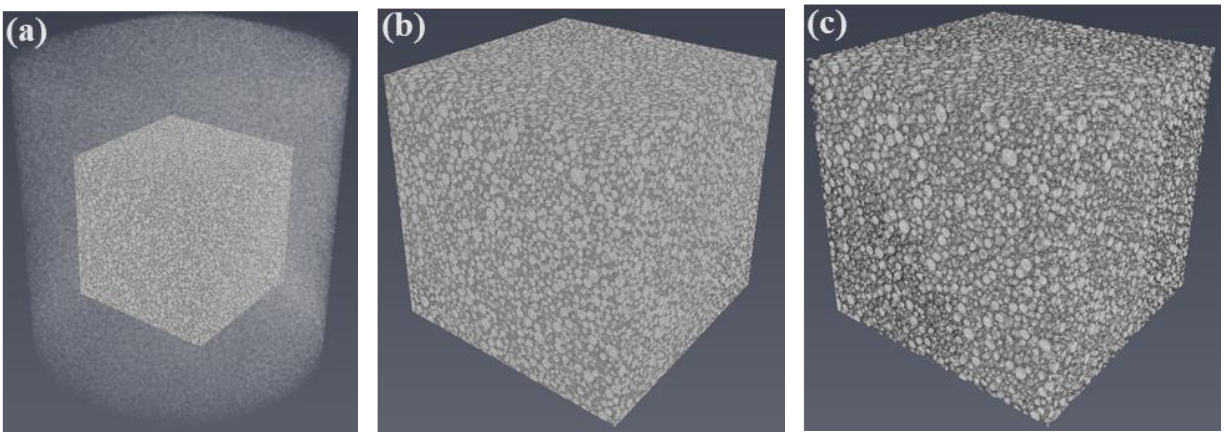

Fig. 5-5 Procedures to process the images, including (a) stacking the image sequence together into a cylinder, (b) extracting a cubic region, and (c) smoothing the images

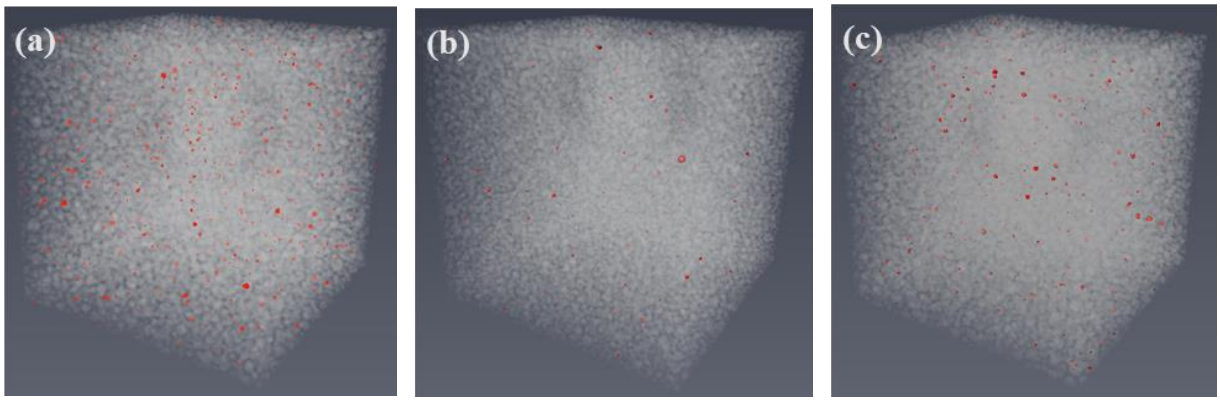

Fig. 5-6 A comparison of the internal porosity of (a) nitrogen atomized powder sample1, (b) nitrogen atomized powder sample2, and (c) argon atomized powder particles

The exist of internal porosity will definitely reduce the true volume of the powder and can further result in lower flow energy. To quantify the different levels of internal porosity in the powders, three regions in each powder sample were extracted, as shown in Fig. 5-7. The number of particles, number of particles with internal porosity, volume of the internal porosity and average volume fraction of the porosity in the particle in these regions were summarized in Table 5-2. Fig. 5-8 shows the volume distribution of the internal porosity and Fig. 5-9 showed the volume fraction

of porosity in particles. The results indicated similar porosity size and volume fraction in the powder samples. The number fraction of particles with porosity in nitrogen atomized powder sample1 is around 4.5 times more than that in nitrogen atomized powder sample2 and 1.5 times more than that in argon atomized powder. With this higher level of internal porosity, the true volume of nitrogen atomized powder sample1 would be lower and less energy is required to make it flow, although avalanche measurements showed it has a lower flowability.

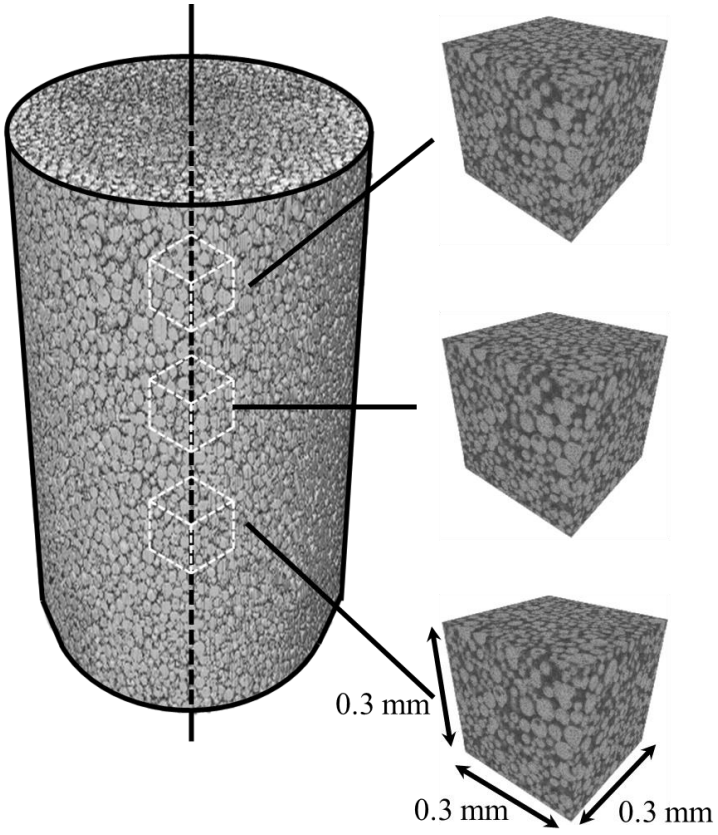

Fig. 5-7 Schematic diagram of 0.3mm×0.3mm×0.3mm regions extracted from powder samples

Table 5-2. Summary of internal porosity measurements made using µCT on powder samples

Atomization gas	**Nitrogen**		**Argon**
Internal porosity quantification	**Sample 1**	**Sample 2**	
Region 1			
Number of particles	800	1219	1074
Number of particles with porosity	36	13	32
Number fraction of particles with porosity	4.5%	1.0%	3.0%
Volume of porosity/Volume of particle	5.9%	4.0%	4.7%
Region 2			
Number of particles	1094	1242	953
Number of particles with porosity	46	10	33
Number fraction of particles with porosity	4.2%	0.8%	3.5%
Volume of porosity/Volume of particle	4.7%	1.9%	5.2%
Region 3			
Number of particles	957	994	934
Number of particles with porosity	44	14	35
Number fraction of particles with porosity	4.6%	1.4%	3.7%
Volume of porosity/Volume of particle	3.7%	3%	6.3%

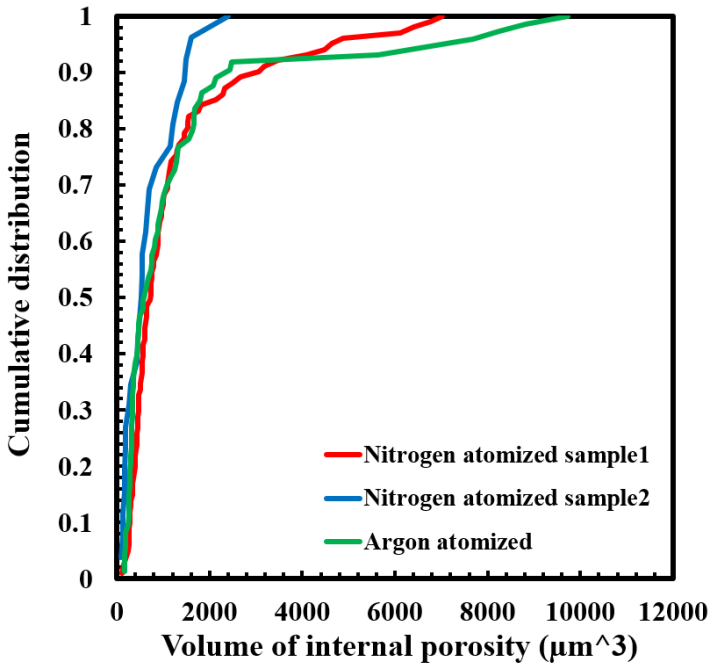

Fig. 5-8 Volume of internal porosity of the powder samples

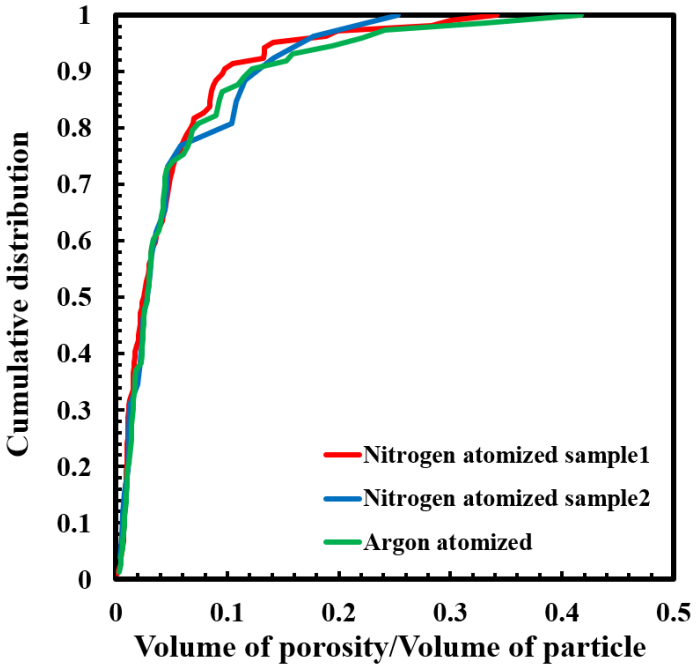

Fig. 5-9 Volume fraction of porosity in particles of the powder samples

5.3 Packing Density and Shear Property

As for conditioned bulk density, the packing forms after conditioning process, which introduces some vibrations to apparent packing [24], so conditioned bulk density is higher than apparent density but still lower than tap density. Compared to shear parameters in RPA, a more general shear testing is the shear cell measurement in the FT4 powder rheometer [63]. Numerous shearing parameters were provided by the assistance of Mohr's circle, as shown in Fig. 5-10. As indicated in Table 5-1. The results showed a similar trend as basic flow energy, which could also be attributed to the different levels of internal porosity, because they share similar physical processes.

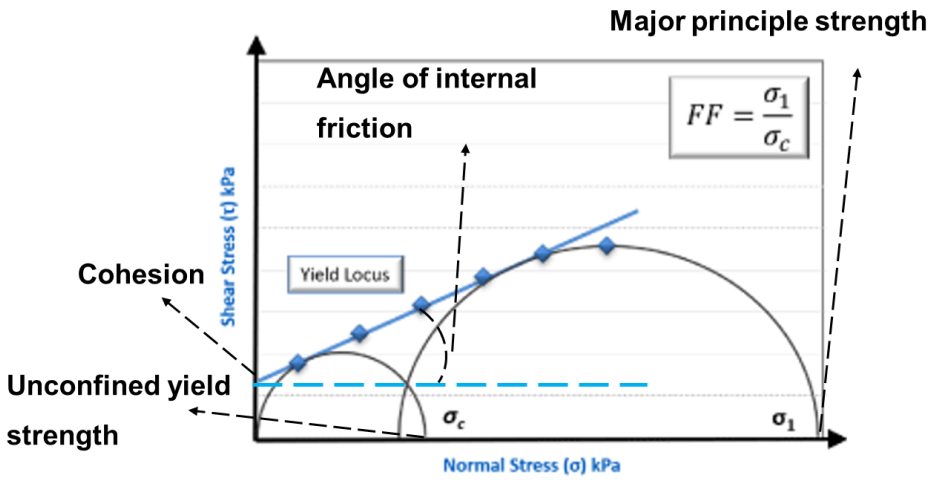

Fig. 5-10 Determination of shear parameters with the help of Mohr's circle of stress

5.4 Permeability

Besides flow energy, permeability was also measured with FT4 powder rheometer, and the results were shown in Fig. 5-11. The permeability of nitrogen atomized powder sample1 was considerably higher than the other two powder samples. Interestingly, the permeability results did not seem to follow the packing density results, in which nitrogen atomized powders have similarly

lower packing density than the argon atomized powder. This means permeability is not completely determined by packing density, so a closer examination on the packing structure inside of powder packing is needed. Previous work showed that permeability of powder bed largely depends on the void size and its distribution [64]. The void size distribution can be estimated from μCT data using Avizo, as shown in Fig. 5-12. The entire void space was separated into small isolated voids based on the distance between particles, and the size of the voids was quantified by calculating the equivalent spherical diameter. The details regarding the algorithm can be found here [62]. It is clearly shown in Fig. 5-13 that the void size in nitrogen atomized powder sample1 is considerably larger than the other two samples, which shows the same trend as the permeability results. This indicates that permeability can be affected by void size rather than completely determined by bulk packing density. There is also a correlation between void size and particle size. As shown in Table 3-2, nitrogen atomized powder sample1 has a slightly larger particle size compared to the other two powder samples, and the same trend was observed in void size of the powders.

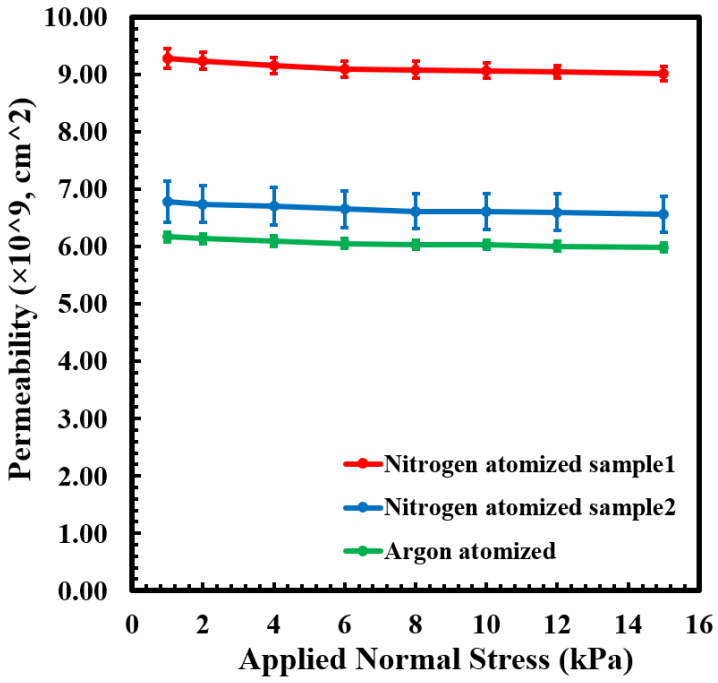

Fig. 5-11. Permeability of three powder samples

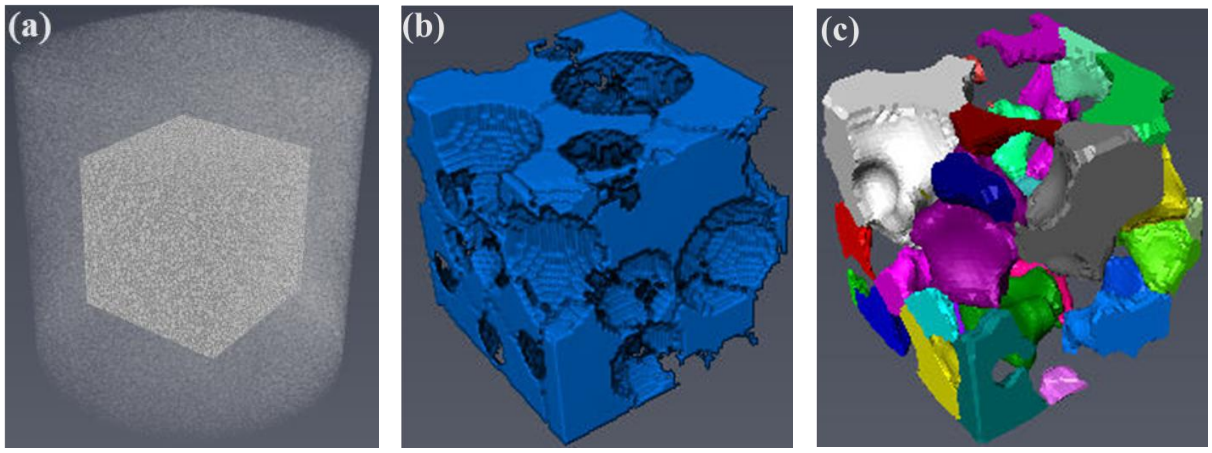

Fig. 5-12 Procedures to estimate void size distribution, including (a) extract a cubic region, (b) conduct material segmentation to separate void space, and (c) divide void space based distance between particle

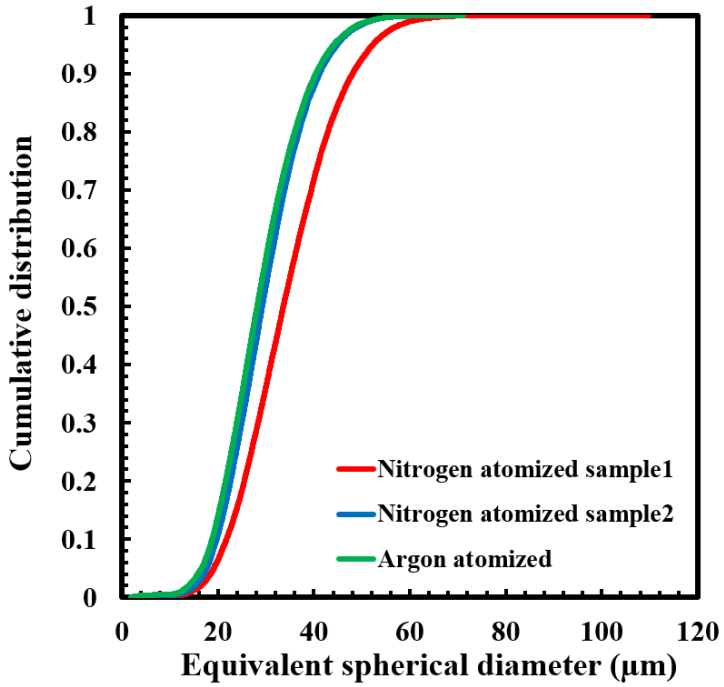

Fig. 5-13. Void size distribution of powder samples

Chapter 6 Summary and Conclusions

The impact of atomization gas, nitrogen or argon, on powder characteristics and rheological properties were investigated with three gas atomized 316L austenitic stainless-steel powders. Particle size distribution of the powders were identified with both laser diffraction and image analysis. The results showed that the particle size distribution of three powders are nearly identical, while particles in nitrogen atomized powder sample1 are slightly larger. Small differences in particle morphology were quantified with convexity, aspect ratio and circularity by image analysis, which were found to be closely related to particle size. Larger particles tend to be less spherical. Compared to argon atomized powder, nitrogen atomized powders exhibited less spherical particle morphology, which could result from different thermal conductivities of nitrogen and argon. Traditional powder characterizations and powder rheology tools were employed to evaluate the flowability and packing density of the powders. Nitrogen atomized powders showed considerably lower flowability and packing density compared to argon atomized powder, which can be correlated to their lower aspect ratio particles. DEM simulations demonstrated that a decrease in aspect ratio can increase the average interparticle force on each particle, and further result in lower flowability, as indicated by higher avalanche angle and break energy. Rheological flow energy is determined by not only interparticle force, but also the true volume of powder. A small reduction in true volume of powder, which results from higher level of internal porosity of particles, can be correlated to a considerable decrease in flow energy, and makes flow energy measurement less sensitive to flowability of powder. Permeability was found to be more dependent on the local void size than bulk packing density, and the difference in void size can be correlated to a small change in particle size.

Overall, it was demonstrated that the selection of atomization gas, nitrogen or argon, impacts the powder characteristics, and different rheological responses were also observed. Besides powder characteristics that generally considered important, such as particle size distribution, a small difference in particle morphology and internal porosity of particles can also affect rheological performance.

Several conclusions could be obtained based on the results:

1) Powders atomized by different gases, nitrogen or argon, present slightly different morphology. Compared to nitrogen atomized powders, argon atomized powder has 10% more spherical particles
2) Compared to nitrogen atomized powders, argon atomized powder showed higher packing density and rheological flowability, which can be correlated to the 10% more spherical particles.
3) DEM simulations revealed that particles with low aspect ratio can result in higher interparticle force, which contributes to lower flowability.
4) There is a strong correlation between internal porosity and basic flow energy measurements. The exist of internal porosity can reduce the true volume of the powder and less energy is needed to make it flow.
5) Permeability of powder bed is more dependent on local void size than bulk packing density.

This work focuses on elucidating the impact of atomization gas on powder characteristic, and the correlation between powder characteristics and rheological responses. Based on this, future work could investigate the AM process performance of these powders, and correlate it to the rheological responses. For example, the quality of powder bed, such as packing density and

uniformity, is largely dependent on the flowability of powder during recoating process. The property of powder bed could be correlated to rheological flowability measurements. Elucidating this correlation will help predict powder behavior in AM process by convenient rheological powder characterization tools. A better understanding on the correlation of powder characteristics, rheological responses and AM process performance is essential to ensure the stability of AM process and improve the quality of final parts. Effective DEM simulations need to be developed to investigate the microscopic response of powder particles under different flow conditions that stimulate complex AM processes.

References

[1] T. DebRoy, H.L. Wei, J.S. Zuback, T. Mukherjee, J.W. Elmer, J.O. Milewski, A.M. Beese, A. Wilson-Heid, A. De, W. Zhang, Additive manufacturing of metallic components – Process, structure and properties, Prog. Mater. Sci., 92 (2018) 112–224.

https://doi.org/10.1016/j.pmatsci.2017.10.001

[2] D.D. Gu, W. Meiners, K. Wissenbach, R. Poprawe, Laser additive manufacturing of metallic components: materials, processes and mechanisms, Int. Mater. Rev., 57 (2012) 133–164.

https://doi.org/10.1179/1743280411Y.0000000014

[3] Silvia Vock, Burghardt Klöden, Alexander Kirchner1, Thomas Weißgärber1, Bernd Kieback, Powders for powder bed fusion: a review, Progress in Additive Manufacturing, 4 (2019) 383–397 https://doi.org/10.1007/s40964-019-00078-6

[4] Metal Additive Manufacturing Industry, https://www.carpenteradditive.com/technical-library/

[5] Gang Chen et al, Shape memory TiNi powders produced by plasma rotating electrode process for additive manufacturing, Trans. Nonferrous Met. Soc. China, 27 (2017) 2647−2655.

https://doi.org/10.1016/S1003-6326(17)60293-0

[6] G. Chen, S.Y.Zhao, P. Tan, J. Wang, C.S.Xiang, H.P. Tang, A comparative study of Ti-6Al-4V powders for additive manufacturing by gas atomization, plasma rotating electrode process and plasma atomization, Powder Technology, 333 (2018) 38-46

https://doi.org/10.1016/j.powtec.2018.04.013

[7] Jayme S. Keist, Todd A. Palmer, Role of geometry on properties of additively manufactured Ti-6Al-4V structures fabricated using laser based directed energy deposition, Materials & Design, 106 (2016) 482-494 https://doi.org/10.1016/j.matdes.2016.05.045

[8] Brian J. Simonds, Edward J. Garboczi, Todd A. Palmer, and Paul A. Williams, Dynamic laser absorptance measured in a geometrically characterized stainless-steel powder layer, Physical review applied, 13 (2020) 024057 https://doi.org/10.1103/PhysRevApplied.13.024057

[9] C. D. Boley, S. A. Khairallah, and A. M. Rubenchik, Calculation of laser absorption by metal powders in additive manufacturing, Appl. Opt., 54 (2015) 2477-2482

http://dx.doi.org/10.1364/AO.54.002477

[10] Salah Eddine Brika, Morgan Letenneur, Christopher Alex Dion and Vladimir Brailovski, Influence of particle morphology and size distribution on the powder flowability and laser powder bed fusion manufacturability of Ti-6Al-4V alloy, Additive Manufacturing, 31 (2020) 100929 https://doi.org/10.1016/j.addma.2019.100929

[11] Vanessa Seyda and Dirk Herzog, Relationship between powder characteristics and part properties in laser beam melting of Ti–6Al–4V, and implications on quality, J. Laser Appl., 29, (2017) 022311 https://doi.org/10.2351/1.4983240

[12] G. Yablokova, M. Speirs, J. Van Humbeeck, J.-P. Kruth, J. Schrooten, R. Cloots, F. Boschini, G. Lumay, J. Luyten, Rheological behavior of β-Ti and NiTi powders produced by atomization for SLM production of open porous orthopedic implants, Powder Technology, 283 (2015) 199–209 https://doi.org/10.1016/j.powtec.2015.05.015

[13] Quy Bau Nguyen, Mui Ling Sharon Nai, Zhiguang Zhu, Chen-Nan Sun, Jun Wei, Wei Zhou, Characteristics of Inconel Powders for Powder-Bed Additive Manufacturing, Engineering, 3 (2017) 695–700 http://dx.doi.org/10.1016/J.ENG.2017.05.012

[14] A. Strondl, O. Lyckfeldt, H. Brodin and U. Ackelid, Characterization and Control of Powder Properties for Additive Manufacturing, JOM, (67) 2015 549-554. https://doi.org/10.1007/s11837-015-1304-0

[15] Venkateshwar Rao Nalluri, Maxim Puchkov, Martin Kuentz, Toward better understanding of powder avalanching and shear cell parameters of drug–excipient blends to design minimal weight variability into pharmaceutical capsules, International Journal of Pharmaceutics, 442 (2013) 49–56 http://dx.doi.org/10.1016/j.ijpharm.2012.08.010

[16] Michael Cornelius Hermann Karg, Alexander Munk, Bhrigu Ahuja, Manuel Veit Backer, Jana Petra Schmitt, Christopher Stengel, Sergey Vyacheslavovich Kuryntsev, Michael Schmidt, Expanding particle size distribution and morphology of aluminium-silicon powders for Laser Beam Melting by dry coating with silica nanoparticles, Journal of Materials Processing Tech., 264 (2019) 155–171 https://doi.org/10.1016/j.jmatprotec.2018.08.045

[17] Zackary Snow, Richard Martukanitz, Sanjay Joshi, On the development of powder spreadability metrics and feedstock requirements for powder bed fusion additive manufacturing, Additive Manufacturing, 28 (2019) 78-86 https://doi.org/10.1016/j.addma.2019.04.017

[18] Amir Mostafaei, Colleen Hilla, Erica L. Stevens, Peeyush Nandwana, Amy M. Elliott, Markus Chmielus, Comparison of characterization methods for differently atomized nickel-based alloy 625 powders, Powder Technology, 333 (2018) 180–192

https://doi.org/10.1016/j.powtec.2018.04.014

[19] Michael J. Heiden, Lisa A. Deibler, Jeff M. Rodelas, Josh R. Koepke, Dan J. Tung, David J. Saiz, Bradley H. Jared, Evolution of 316L stainless steel feedstock due to laser powder bed fusion process, Additive Manufacturing, 25 (2019) 84–103 https://doi.org/10.1016/j.addma.2018.10.019

[20] J. A. Slotwinski, E. J. Garboczi, P. E. Stutzman, C. F. Ferraris, S. S. Watson, and M. A. Peltz, Characterization of Metal Powders Used for Additive Manufacturing, Journal of Research of the National Institute of Standards and Technology, 119 (2014) 460-493

http://dx.doi.org/10.6028/jres.119.018

[21] Jose Alberto Muñiz-Lerma, Amy Nommeots-Nomm, Kristian Edmund Waters, Mathieu Brochu, A Comprehensive Approach to Powder Feedstock Characterization for Powder Bed Fusion Additive Manufacturing: A Case Study on AlSi7Mg, Materials, 11 (2018) 2386

https://doi.org/10.3390/ma11122386

[22] Ross Cunningham, Andrea Nicolas, John Madsen, Eric Fodran, Elias Anagnostou, Michael D. Sangid and Anthony D. Rollett, Analyzing the effects of powder and post-processing on porosity and properties of electron beam melted Ti-6Al-4V, Mater. Res. Lett., 5 (2017) 516-525 https://doi.org/10.1080/21663831.2017.1340911

[23] R.M. German, Powder Metallurgy and Particulate Materials Processing, 2005.

[24] ASTM B213, Standard Test Methods for Flow Rate of Metal Powders Using the Hall Flowmeter, ASTM International, West Conshohocken, PA, 2017 https://doi:10.1520/B0213-17.2.

[25] ASTM B212, Standard Test Method for Apparent Density of Free-Flowing Metal Powders Using the Hall Flowmeter Funnel, ASTM International, West Conshohocken, PA, 2013

https://doi:10.1520/B0212-13.

[26] ASTM B527, Standard Test Method for Tap Density of Metal Powders and Compounds, ASTM International, West Conshohocken, PA, 2015 https://doi:10.1520/B0527-15.

[27] J. Clayton, D. Millington-Smith, B. Armstrong, The Application of Powder Rheology in Additive Manufacturing, JOM, 67 (2015) 544–548. https://doi.org/10.1007/s11837-015-1293-z

[28] Z.R. Khayat, T.A. Palmer, Impact of iron composition on the properties of an additively manufactured solid solution strengthened nickel base alloy, Materials Science & Engineering A, 718 (2018) 123–134 https://doi.org/10.1016/j.msea.2018.01.112

[29] S.D. Meredith, J.S. Zuback, J.S. Keist, T.A. Palmer, Impact of composition on the heat treatment response of additively manufactured 17–4 PH grade stainless steel, Materials Science & Engineering A, 738 (2018) 44–56 https://doi.org/10.1016/j.msea.2018.09.066

[30] ASTM F3049-14, Standard Guide for Characterizing Properties of Metal Powders Used for Additive Manufacturing Processes, ASTM International, West Conshohocken, PA, 2014

https://doi: 10.1520/F3049-14

[31] G. K. Khoe, T. L. Ip and J. R. Grace, Rheological and fluidization behaviour of powders of different particle size distribution, Powder Technology, 66 (1991) 127-141

https://doi.org/10.1016/0032-5910(91)80094-Y

[32] D. Gauthier, S. Zerguerras, G. Flamant, Influence of the particle size distribution of powders on the velocities of minimum and complete fluidization, Chemical Engineering Journal, 74 (1999) 181-196 https://doi.org/10.1016/S1385-8947(99)00075-3

[33] Yun Bai, Grady Wagner and Christopher B. Williams, Effect of Particle Size Distribution on Powder Packing and Sintering in Binder Jetting Additive Manufacturing of Metals, Journal of Manufacturing Science and Engineering, 139 (2017) 081019 1-6

https://doi.org/10.1115/1.4036640

[34] K. Vollmari, R. Jasevičius, H. Kruggel-Emden, Experimental and numerical study of fluidization and pressure drop of spherical and non-spherical particles in a model scale fluidized bed, Powder Technology, 291 (2016) 506–521 https://doi.org/10.1016/j.powtec.2015.11.045

[35] Berenika Hausnerova, Bhimasena Nagaraj Mukund, Daniel Sanetrnik, Rheological properties of gas and water atomized 17-4PH stainless steel MIM feedstocks: Effect of powder shape and size, Powder Technology, 312 (2017) 152–158 https://doi.org/10.1016/j.powtec.2017.02.023

[36] M. Leturia, M. Benali, S.Lagarde, I. Ronga, K. Saleh, Characterization of flow properties of cohesive powders: A comparative study of traditional and new testing methods, Powder Technology, 253 (2014) 406–423 http://dx.doi.org/10.1016/j.powtec.2013.11.045

[37] Albert W. Alexander, Bodhisattwa Chaudhuri, AbdulMobeen Faqih, Fernando J. Muzzio, Clive Davies, M. Silvina Tomassone, Avalanching flow of cohesive powders, Powder Technology, 164 (2006) 13–21 https://doi.org/10.1016/j.powtec.2006.01.017

[38] Qin Li, Victor Rudolph, Bernhard Weigl, Alan Earl, Interparticle van der Waals force in powder flowability and compactibility, International Journal of Pharmaceutics, 280 (2004) 77–93 https://doi.org/10.1016/j.ijpharm.2004.05.001

[39] H.P. Tang, M. Qian, N. Liu, X.Z. Zhang, G.Y. Yang and J. Wang, Effect of Powder Reuse Times on Additive Manufacturing of Ti-6Al-4V by Selective Electron Beam Melting, JOM, 67 (2015) 555-563. https://doi.org/10.1007/s11837-015-1300-4

[40] Shuji Matsusaka and Hiroaki Masuda, Electrostatics of particles, Advanced Powder Technol., 14 (2003) 143-166 https://doi.org/10.1163/156855203763593958

[41] Ramon Cabiscol, Jan Henrik Finke, Arno Kwade, Calibration and interpretation of DEM parameters for simulations of cylindrical tablets with multi-sphere approach, Powder Technology, 327 (2018) 232–245 https://doi.org/10.1016/j.powtec.2017.12.041

[42] Xiangwu Xiao, Yuanqiang Tan, Hao Zhang, Rong Deng, Shengqiang Jiang, Experimental and DEM studies on the particle mixing performance in rotating drums: Effect of area ratio, Powder Technology, 314 (2017) 182–194 http://dx.doi.org/10.1016/j.powtec.2017.01.044

[43] C.J. Coetzee, Calibration of the discrete element method and the effect of particle shape, Powder Technology, 297 (2016) 50–70 http://dx.doi.org/10.1016/j.powtec.2016.04.003

[44] Prathamesh S. Desai, Akash Mehta, Patrick S.M. Dougherty, C. Fred Higgs III, A rheometry based calibration of a first-order DEM model to generate virtual avatars of metal Additive Manufacturing powders, Powder Technology, 342 (2019) 441–456

https://doi.org/10.1016/j.powtec.2018.09.047

[45] C. Hare, U. Zafar, M. Ghadiri, T. Freeman, J. Clayton, M. J. Murtagh, Analysis of the dynamics of the FT4 powder rheometer, Powder Technology, 285 (2015) 123–127

http://dx.doi.org/10.1016/j.powtec.2015.04.039

[46] Z. Y. Zhou, R. P. Zou, D. Pinson, A. B. Yu, Angle of repose and stress distribution of sandpiles formed with ellipsoidal particles, Granular Matter, 16 (2014) 695–709

https://doi.org/10.1007/s10035-014-0522-4

[47] Xiao Liang Deng and Rajesh N. Davé, Dynamic simulation of particle packing influenced by size, aspect ratio and surface energy, Granular Matter, 15 (2013) 401–415

https://doi.org/10.1007/s10035-013-0413-0

[48] ASTM Standard E1019-08, Standard test methods for determination of carbon, sulfur, nitrogen, and oxygen in steel, iron, nickel, and cobalt alloys by various combustion and fusion techniques, (2008). https://doi:10.1520/E1019-11.

[49] ASTM Standard E1479, Standard Practice for Describing and Specifying Inductively-Coupled Plasma, (2013). https://doi:10.1520/E1479-99R11.2.

[50] ASTM Standard A240, Standard Specification for Chromium and Chromium-Nickel Stainless Steel Plate, Sheet and Strip for Pressure Vessels and for General Applications, I (2004) https://doi:10.1520/A0240.

[51] ASTM Standard B822, Standard Test Method for Particle Size Distribution of Metal Powders and Related Compounds by Light Scattering, (2001). https://doi:10.1520/B0822-10.2.

[52] A. B. Spierings, M. Voegtlin, T. Bauer, K. Wegener, Powder flowability characterization methodology for powder-bed-based metal additive manufacturing, Progress in Additive Manufacturing, 1 (2016) 9-20. https://doi: 10.1007/s40964-015-0001-4

[53] Martin Allen, Gareth J. Brown, Nick J. Miles, Measurement of boundary fractal dimensions: review of current techniques, Powder Technology, 84 (1995) 1-14. https://doi:10.1016/0032-5910(94)02967-S

[54] Hoshino, T., Mito, K., Nagashima, A. et al. Determination of the thermal conductivity of argon and nitrogen over a wide temperature range through data evaluation and shock-tube experiments, Int J Thermophys., 7 (1986) 647-662. https://doi:10.1007/BF00502397

[55] C. Kloss, C. Goniva, A. Hager, S. Amberger, S. Pirker, Models, algorithms and validation for opensource DEM and CFD-DEM, Prog. Comput. Fluid Dy., 12 (2012) 140–152.

https://www.researchgate.net/profile/Stefan_Pirker/publication/264439676_Models_algorithms_and_validation_for_opensource_DEM_and_CFD-DEM/links/56af5af108ae28588c62fd16.pdf

[56] Mindt, H.W., Megahed, M., Lavery, N.P. et al. Powder Bed Layer Characteristics: The Overseen First-Order Process Input, Metall and Mat Trans A, 47 (2016) 3811-3821. https://doi:10.1007/s11661-016-3470-2

[57] O'Sullivan, Catherine, Particulate Discrete Element Modelling, Applied Geotechnics, 4 (2014) 79-87.

[58] Jun Ai, Jian-Fei Chen, J. Michael Rotter, Jin Y. Ooi, Assessment of rolling resistance models in discrete element simulations, Powder Technology, 206 (2011) 269–282

https://doi:10.1016/j.powtec.2010.09.030

[59] S. Geer, M. L. Bernhardt-Barry, E. J. Garboczi, J. Whiting, A. Donmez, A more efficient method for calibrating discrete element method parameters for simulations of metallic powder

used in additive manufacturing, Granular Matter, 20 (2018) 77. https://doi:10.1007/s10035-018-0848-4

[60] S. Haeri, Y.Wang, O. Ghita, J.Sun, Discrete element simulation and experimental study of powder spreading process in additive manufacturing, Powder Technology, 306 (2016) 45–54.

https://doi:10.1016/j.powtec.2016.11.002

[61] Schindelin, J.; Arganda-Carreras, I.; Frise, E.; Kaynig, V.; Longair, M.; Pietzsch, T.; Preibisch, S.; Rueden, C.; Saalfeld, S.; Schmid, B. Fiji: An open-source platform for biological-image analysis. Nat. Methods, 9 (2012) 676–682. https://doi:10.1038/nmeth.2019

[62] Thermo Scientific Avizo Software 9 User's Guide

https://assets.thermofisher.com/TFS-Assets/MSD/Product-Guides/user-guide-avizo-software.pdf

[63] T. Freeman, J. Clayton, B. Armstrong, F. Technology, M. Court, The Rheology of Powders and Bulk Materials – a Multivariate Approach Using Dynamic, Shear and Bulk Property Measurements, Annu. Transations Nord. Rheol. Soc., 21 (2013) 83–90.

https://nrs.blob.core.windows.net/pdfs/nrspdf-419a34b1-e6b5-43df-91d6-a51fdc1e6b6c.pdf.

[64] Shoichiro Hamamoto, Per Moldrup, Ken Kawamoto, Toshihiro Sakaki, Taku Nishimura, Toshiko Komatsu, Pore network structure linked by X-ray CT to particle characteristics and transport parameters, Soils and Foundations, 56 (2016) 676–690.

https://doi:10.1016/j.sandf.2016.07.008